For Chemistry — An Asian Journal

Design and Synthesis of Far-Red to Near-Infrared Chromophores with Pyrazine-Based Boron Complexes

Hiromasa Takahashi, Dr. Hiroyuki Watanabe, Dr. Shunichiro Ito, Prof. Dr. Kazuo Tanaka and Prof. Dr. Yoshiki Chujo*

Department of Polymer Chemistry, Graduate School of Engineering, Kyoto University, Katsura, Nishikyo-ku, Kyoto 615-8510, Japan

E-mail: tanaka@poly.synchem.kyoto-u.ac.jp

HP: https://poly.synchem.kyoto-u.ac.jp

Abstract

We synthesized new binuclear boron complexes based on pyrazine with *ortho* and *para* substitution patterns. It was demonstrated that the *para*-linked complexes possess a significantly narrow energy gap between highest occupied and lowest unoccupied molecular orbitals (HOMO and LUMO), leading to their far-red to near-infrared emission properties. Meanwhile, the ortho-substituted complex showed orange emission. Considering the HOMO and LUMO distributions of pyrazine, the boron complexation to the nitrogen atoms would stabilize its LUMO more efficiently than its HOMO because a nodal plane in the HOMO passes through the two nitrogen atoms. The theoretical study suggests that the *para*-substitution would not significantly perturb such a characteristic HOMO distribution originating from pyrazine in stark contrast to the *ortho*-substituted one. As a result, the HOMO–LUMO gap of the *para*-linked complex is dramatically narrower than that of the *ortho*-linked one.

Introduction

Far-red and near-infrared (FR/NIR) light, which involves the wavelength ranging between 700 to 750 nm and 750 to 2500 nm, respectively, composes more than 50% of the energy of the solar radiation received at the surface of the earth,[1] and can penetrate deeper into biological tissues.[2] Therefore, recent years have witnessed the development of organic FR/NIR absorbers and emitters for the key components of photovoltaic cells,[3,4] light-emitting diodes,[5] bio-imaging materials,[6,7] and photocleavable protecting groups.[8] For applying to bio-imaging materials in particular, large Stokes shifts are required because of a demand for avoiding self-reabsorption and inner filter effect, while many common NIR emitters based on cyanines and rhodamines show small Stokes shifts (< 1000 cm^{-1}).[9,10] Therefore, there is still much room for the development of NIR chromophores providing large Stokes shifts.[11]

The energy gap (E_g) between highest occupied and lowest unoccupied molecular orbitals (HOMO and LUMO) of π-conjugated molecules characterizes their absorption and emission wavelengths. The typical strategies for obtaining FR/NIR chromophores, *i.e.*, narrow E_g would be classified into three types as follows: extension of π-conjugation systems,[12,13] enhancement of the donor–acceptor interaction by substituents,[14] and introduction of heteroatoms.[15,16] Selective modulations of frontier molecular orbital (FMO) energies and symmetries have been reported for pyridine,[17] pyrenes,[18–23] helicenes,[24–26] boron dipyrromethenes (BODIPYs),[27] and azaphenalenes[28–32] to control their photophysical and photochemical properties.

Among heteroatom-containing π-conjugated systems, π-conjugated systems containing boron have been widely reported. Generally, the coordination of boron stabilizes the orbital energy of the corresponding ligands because the electron density of the coordinated site should be lowered by the complexation.[33] When the LUMO of a compound possesses a larger orbital contribution from

the atom to which boron binds than its HOMO, the boron complexation should lower the LUMO energy level more effectively than the HOMO level.[34]

In this work, we conceived that a pyrazine-based scaffold would be suitable for constructing FR/NIR chromophores. Starting from benzene, each of the HOMO (e_{1g}) and LUMO (e_{2u}) doubly degenerates (Figure 1). The replacement of the diagonal pair of CH groups by nitrogen atoms gives pyrazine (D_{2h} symmetry). The FMOs of benzene with symmetry species e_{1g} and e_{2u} split into the four FMOs of pyrazine with symmetry species b_{2g}, b_{1g}, b_{3u} and a_u. It is because b_{2g} and b_{3u} FMOs of pyrazine possess large contributions from the $2p_z$ orbitals of nitrogen, whereas a nodal plane passes through the diagonal nitrogen atoms for the a_u and b_{1g} FMOs. As a result, the b_{1g} and b_{3u} FMOs of pyrazine exhibit the desired, partly non-overlapped HOMO/LUMO distributions for realizing the selective stabilization of LUMO by boron complexation to give FR/NIR chromophores. In order to assess this molecular design, we synthesized a series of binuclear boron complexes with both *para* and *ortho*-substitution patterns. In this discussion, we focused only on the π orbitals and ignored the lone pair orbital of pyrazine (a_g), because it would be away from the frontier orbital band after boron complexation.

Recently, Fang and co-workers have developed pyrazine-based boron complexes with NIR photophysical properties (λ_{abs} ~ 700–820 nm).[35] In their work, the complexation of the boron atoms and the pyrazine moiety was considered as a tool to enhance the planarity of the molecule and the electron-withdrawing property of pyrazine. They argued that the boron atoms contribute to the efficient extension of π-conjugated systems and the enhancement of donor-acceptor interaction, which are common molecular design strategy for NIR chromophores as mentioned above. However, they have not evaluated the effects of substitution patterns on the optical properties. Additionally, double [5]helicenes with a pyrazine-diboron core was reported by Oda,

Hatakeyama and co-workers.[36] These twisted complexes exhibited the absorption and emission in the shorter-wavelength region (λ_{abs} ~ 550–570 nm, λ_{em} ~ 620–650 nm) than the complexes developed by Fang *et al*. Therefore, it is still important to reveal the effects of substitution patterns on the photophysical properties of the pyrazine-based boron complexes.

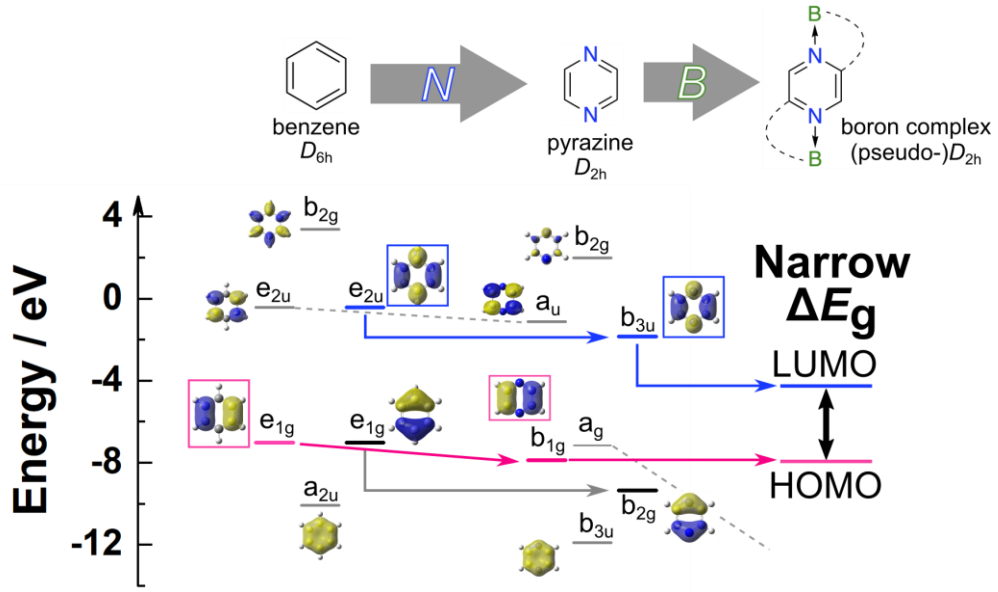

Figure 1. Molecular design for NIR chromophores. Kohn–Sham molecular orbital energies of benzene and pyrazine were calculated at the B3LYP/6-31+G(d,p) level of theory. Orbital distributions are shown with 0.035 of isovalue. Each energy level was labeled with the symmetry species.

Results and Discussion

Binuclear diarylboron complexes **para-B**, **para-BMeO**, and **ortho-B** were synthesized according to Scheme 1. The corresponding dimethylpyrazines were deprotonated by lithium diisopropylamide (2 eq.), followed by the reaction with the corresponding Weinreb amides (**1a** and **1b**) to afford the ligands **para-L** and **para-LMeO**. Subsequent boron complexations of the ligands were accomplished by the reactions with dimesitylfluoroborane in the presence of triethylamine. The chemical structures of the boron complexes were confirmed by ^{1}H, $^{11}B\{^{1}H\}$, and $^{13}C\{^{1}H\}$ NMR spectroscopy (Figures S11–S16 and S20–S22) and high-resolution mass spectrometry. ^{1}H NMR spectra of the ligands showed the characteristic peaks attributable to the keto and enol forms (Figures S5–S10 and S17–S19). All three complexes were soluble in common organic solvents, such as toluene, chloroform, dichloromethane (DCM), dimethylsulfoxide (DMSO), and 2-methyltetrahydrofuran (2Me-THF). The complexes were stable enough to be subjected photophysical measurements under ambient condition, while the low isolated yields were mainly due to the instability of the complexes to silica gel.

Scheme 1. Synthetic scheme of pyrazine-based boron complexes

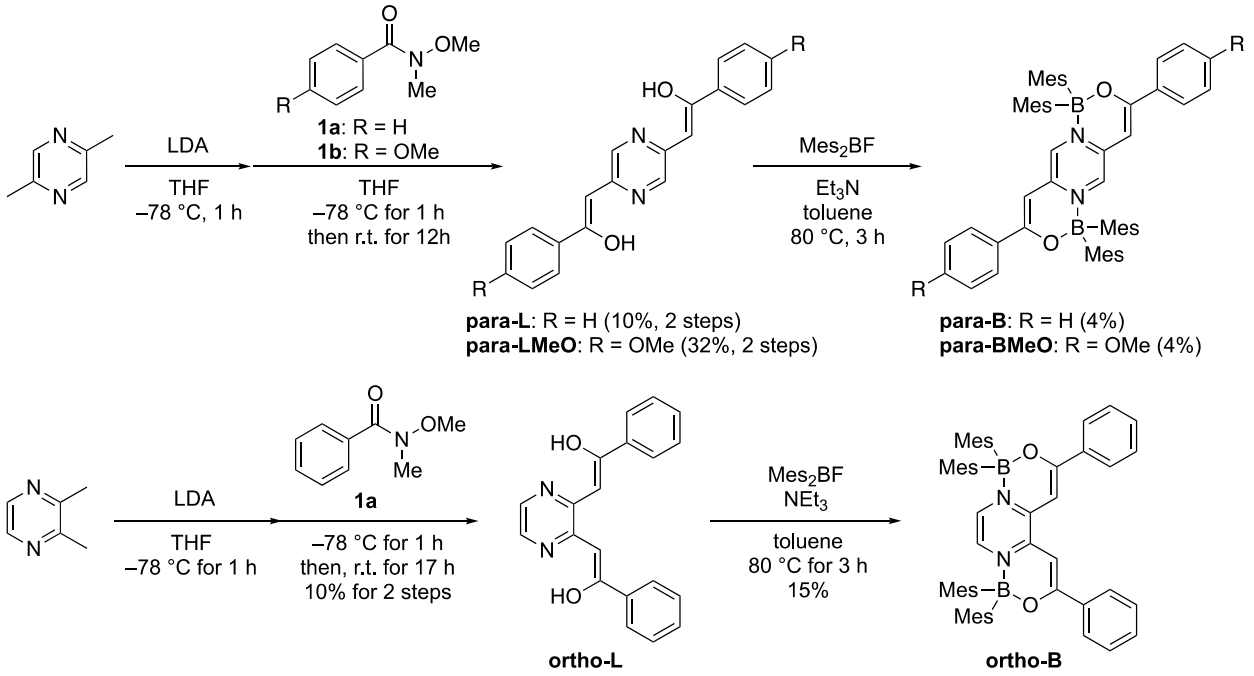

UV–vis absorption and photoluminescence (PL) spectra of the synthesized complexes and ligands were recorded in toluene (Figure 2a and Table 1). The concentration (1.0×10^{-5} M) was dilute enough to ignore the self-absorption effect. The boron complexation induced the bathochromic shift of the longest-wavelength absorption bands for both *para*- and *ortho*-substitution patterns. The resulting *para*-substituted complexes exhibited a strong absorption band reaching the red to far-red region. In stark contrast, the longest-wavelength absorption of the *ortho* counterpart was observed in the shorter wavelength region than those of the *para* ones. Most importantly, the PL spectra of **para-B** and **para-BMeO** were observed in the FR/NIR region, while almost the whole PL band of **ortho-B** was in the visible region. These results indicate that the *para*-substitution is appropriate to achieve a longer-wavelength absorption and emission. It should be noted that the apparent difference in the absorption spectra between the ligands could originate from their keto-enol tautomerization of the ligands.

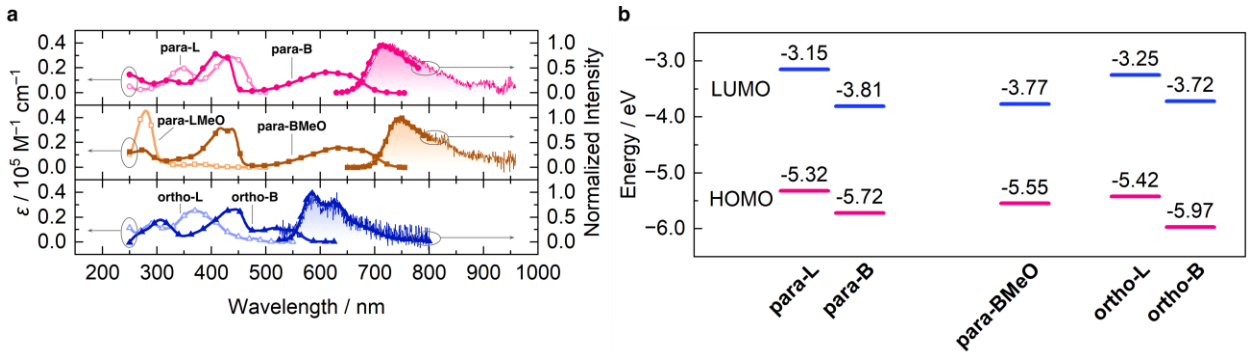

Figure 2. (a) UV–vis absorption (left axis) and PL (right axis) spectra of synthesized boron complexes and their corresponding ligands in toluene (1.0×10^{-5} M). Legends: Thick line with solid symbols, absorption and PL of complexes recorded with a fluorescence spectrometer; thick line with open symbols, absorption of ligands; thin line with a shade, PL of complexes recorded with an absolute quantum yield spectrometer. (b) Orbital energy diagram estimated by cyclic voltammetry with the following empirical formula: E_{HOMO} / eV = –5.1 – $E_{ox,CV}$ / V, E_{LUMO} = –5.1 – $E_{red,CV}$ / V, where $E_{ox,CV}$ and $E_{red,CV}$ are the onset potentials of first oxidation and reduction peaks, respectively.

Table 1. Optical properties of synthesized boron complexes

	Condition	λ_{abs} / nm[a]	λ_{em} / nm[b]	Stokes shift / cm^{-1}	Φ_{PL}[c]
para-B	Toluene	621	718	2,200	0.05
	2Me-THF	621	720	2,200	0.04
	DCM	613	715	2,300	0.05
	DMSO/DCM[d]	618	722	2,300	0.04
	Solid	n.d.	761[e]	n.d.	0.03
para-BMeO	Toluene	641	739	2,100	0.04
	2Me-THF	639	743	2,200	0.03
	DCM	632	741	2,300	0.03
	DMSO/DCM[d]	640	750	2,300	0.03
	Solid	n.d.	788[f]	n.d.	0.02
ortho-B	Toluene	515	584	2,300	0.02
	2Me-THF	516	584	2,300	0.02
	DCM	516	584	2,300	0.01
	DMSO/DCM[d]	519	587	2,100	0.03
	Solid	n.d.	615	n.d.	0.06

[a]Absorption maximum in the longest wavelength region (concentration: 1.0×10^{-5} M). [b]Fluorescence maxima excited at λ_{abs} for each condition. [c]Absolute quantum yield determined with an integrating sphere with excitation at λ_{abs}. [d]DMSO/DCM = 99/1 (vol/vol). [e]Fluorescence maxima excited at 618 nm. [f]Fluorescence maxima excited at 641 nm. n.d.: Not determined.

The absolute quantum efficiencies (Φ_{PL}) of **para-B** and **para-BMeO** were determined to be 0.05 and 0.04 in toluene, respectively. These values are comparable to those of other NIR-emissive

molecules with relatively large Stokes shifts (> 2000 cm^{-1}), which are large enough for bio-imaging applications, measured in polar solvents.[37,38] Importantly, the absorption and emission behaviours of the complexes were not remarkably affected by the kind of solvents, indicating that the S_1 states of these complexes could be assigned to a locally excited state rather than an intramolecular charge transfer one. Additionally, the solids of **para-B** and **para-BMeO** emit NIR light with keeping Φ_{PL} values (Φ_{PL}^{solid}: 0.03 for **para-B**; 0.02 for **para-BMeO**). Furthermore, the enhanced Φ_{PL} value of the solid of **ortho-B** indicates its aggregation-induced emission enhancement (AIEE) property. Related boron complexes with *N*,*O*-type ligands often showed such AIEE property.[39–41] The solid-state emission spectrum of **ortho-B** showed an apparent vibrational structure, while those of the other para-complexes were broad (Figure S26). These results suggest that intermolecular interactions in the solid state of **ortho-B** might be weaker than those of the other complexes. Therefore, the restriction of molecular motions by the aggregation might be a more dominant effect for **ortho-B**, resulting in the AIEE behavior. The sterically hindered mesityl groups, which are located at the same molecular face of **ortho-B**, might expel strong intermolecular interactions which cause the non-radiative quenching of exciton energy. Unfortunately, the low crystallinity of these complexes hampered us from obtaining further insights into their packing structures and intermolecular interactions.

The HOMO and LUMO levels of the complexes were estimated using cyclic voltammetry with the redox couple of ferrocene/ferrocenium as an external standard (Figures 2b and S27).[42] The boron complexation effectively lowered the LUMO energy (**para-L**, –3.15 eV; **para-B**, –3.81 eV). Meanwhile, the HOMO energy was stabilized less efficiently than the LUMO (**para-L**, –5.32 eV; **para-B**, –5.72 eV). As a result, the E_g of **para-B** was significantly narrower than that of **para-L**. On the other hand, in the case of the ortho derivative, the HOMO was stabilized to a similar extent

with the LUMO. Consequently, **ortho-B** exhibited the higher-energy absorption and emission than **para-B**. It is worth noting that the keto–enol tautomerization might affect the results of the CV measurements. The ideal enol-enol forms could possess a higher HOMO and a lower LUMO than the other forms (enol-keto and keto-keto forms) because of the extended π-conjugation. Particularly, we were not able to precisely determine the redox potentials of the ligand **para-LMeO** likely because of the tautomerization.

To evaluate the photophysical and electrochemical properties, we performed density functional theory (DFT) and time-dependent DFT (TD-DFT) calculations at the B3LYP/6-31+G(d,p) level of theory using the Gaussian 16 package.[43] The several benchmark calculations indicated that the above-mentioned level of theory was optimal for evaluating this class of complexes (Table S31). The enol-enol form of each ligand was employed for assessing the effects of the boron complexation. The calculation results for the other forms are shown in the Supporting Information. The Kohn–Sham HOMOs and LUMOs are shown in Figure 3. Notably, the HOMO and LUMO distributions of the *para*-substituted ligands and complexes were similar to those of pyrazine despite a small contribution of the nitrogen atoms of pyrazine ring to the HOMO. The calculated orbital contributions from the nitrogen atom to the whole HOMO were 1.8% for **para-B**. Therefore, the boron-complexation led to the more efficient stabilization of the LUMO than the HOMO, resulting in the far-red to NIR emission. On the other hand, the HOMO of **ortho-B** was significantly distributed on these nitrogen atoms (contribution: 5.3%). The boron complexation lowered the HOMO by 0.25 eV, which was larger than the value for **para-B** (0.16 eV). It is worth noting that the *para*- and *ortho*-derivatives exhibited no significant difference in molecular planarity (Figure S28). Hence, the difference in the efficiency of π-conjugation could hardly affect the optical and electronic properties of these complexes. The TD-DFT calculations reproduced the

lower-energy electronic transition (S_0–S_1) of **para-B** (634 nm) and **para-BMeO** (686 nm) than that of **ortho-B** (536 nm). The S_1 state of all complexes are assigned to the HOMO–LUMO transition (see the Supporting Information). Their HOMO and LUMO are mainly located at the central pyrazine ring, indicating the locally excited character of the S_1 state, as experimentally confirmed.

Overall, we concluded that the difference in the HOMO distribution between the *para*- and *ortho*-derivatives should be mainly responsible for the change in the optical properties. The HOMO of the *ortho* system completely differs from those of the other complexes because of the complete disappearance of a C_2 axis perpendicular to the pyrazine plane. In contrast, the π-conjugation systems of **para-B** and **para-BMeO** maintain such a C_2 axis. In addition, the through-space in-phase (bonding) interaction between the π-orbitals of enol units might stabilize the HOMO of **ortho-B**. Such interactions are absent in the *para*-systems because the enol units are apart from each other.

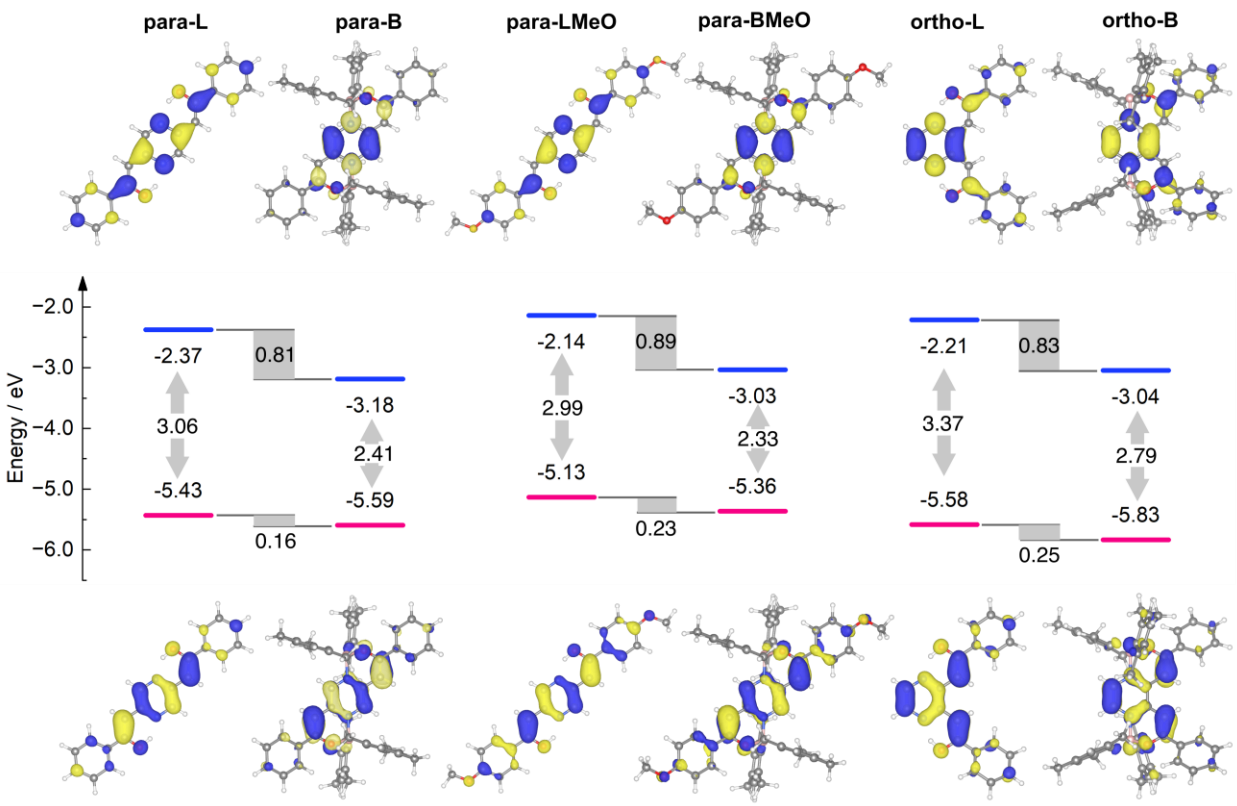

Figure 3. FMO diagrams and Kohn–Sham HOMO (magenta) and LUMO (blue) distributions of the complexes and ligands. Isovalues are set at 0.03. Legends: Gray, carbon; white, hydrogen; pink, boron; blue, nitrogen; red, oxygen.

Additionally, the HOMO level of **para-BMeO** was apparently higher than that of **para-B**. Meanwhile, there was only a limited difference in LUMO levels between them (Figures 2b and 3). This different effect of the methoxy groups at the *para*-positions lead to the narrower E_g of **para-BMeO**, resulting in the bathochromic shift of the absorption and PL spectra. The larger change in the HOMO energy should be derived from the larger contribution from the *para*-carbon atoms to the HOMO. The LUMOs of **para-B** and **para-BMeO** showed no apparent contribution from these *para*-carbon atoms. Thus, the electron-donating methoxy groups of **para-BMeO** should raise the HOMO energy more efficiently.

Conclusion

We successfully obtained the pyrazine-based far-red to NIR-emissive boron complexes whose E_g are efficiently narrowed by boron coordination. *Para*- and *ortho*-substituted complexes were synthesized to evaluate the effects of substitution patterns. This study demonstrates that the *para*-substitution is more suitable for constructing the far-red to NIR emitters than the *ortho*-substitution. The boron complexation stabilized the LUMO of the *para*-substituted complexes more efficiently than that of the HOMO. Meanwhile, the HOMO of the *ortho* complex was more significantly lowered by the complexation than that of *para* one. The C_2 symmetry axis perpendicular to the pyrazine ring in the *para* complexes should be responsible for maintaining the orbital characters coming from pyrazine and, thus, their FR/NIR absorption and emission properties.

Experimental Section

Materials: Tetrahydrofuran (THF) and triethylamine (NEt_3) were purified using a two-column solid-state purification system (Glasscontour System, Joerg Meyer, Irvine, CA). Reagents (*N*,*O*-dimethylhydroxylamine hydrochloride, benzoyl chloride, $NaHCO_3$, Na_2SO_4, *p*-methoxybenzoyl chloride, lithium diisopropylamide (LDA), 2,5-dimethylpyrazine, dimesitylfluoroborane) and solvents (dichloromethane (DCM), methanol, toluene, *n*-hexane) were purchased from commercial sources and used without further purification.

Synthesis of 1a:[44] To a solution of *N*,*O*-dimethylhydroxylamine hydrochloride (9.76 g, 100 mmol) in anhydrous DCM (250 mL) were added benzoyl chloride (11.6 mL, 100 mmol) and NEt_3 (28.0 mL, 202 mmol) and at 0 °C. The reaction mixture was stirred at room temperature for 1 h and quenched with saturated $NaHCO_3$ (150 mL). DCM (50 mL) was added to extract the product from the aqueous layer. The organic layer was washed with brine (60 mL), dried over anhydrous Na_2SO_4, filtered and concentrated to afford the crude product **1a** (12 g, 74% crude yield).

^{1}H NMR ($CDCl_3$, ppm): δ 7.66 (2H, d, J = 6.7 Hz), 7.42 (3H, m), 3.55 (3H, s), 3.36 (3H, s) ppm.

^{13}C NMR ($CDCl_3$, ppm): δ 134.0, 130.4, 128.0, 127.9, 60.9, 33.6 ppm.

HRMS (p-ESI) calcd for $C_9H_{11}NO_2$+Na $[M+Na]^+$ 168.0682, found 168.0679.

Synthesis of 1b:[44] To a solution of *N*,*O*-dimethylhydroxylamine hydrochloride (9.76 g, 100 mmol) in anhydrous DCM (200 mL) were added *p*-methoxybenzoyl chloride (13.5 mL, 100 mmol) and NEt_3 (28.0 mL, 202 mmol) and at 0 °C. The reaction mixture was stirred at room temperature for 1 h and quenched with saturated $NaHCO_3$ (150 mL). (DCM (50 mL) was added to extract the product from the aqueous layer.) The organic layer was washed with brine (70 mL), dried over

anhydrous Na_2SO_4, filtered and concentrated to afford the crude product **1b** (13 g, 69% crude yield).

^{1}H NMR ($CDCl_3$, ppm): δ 7.72 (2H, d, *J* = 8.9 Hz), 6.89 (2H, d, *J* = 8.9 Hz), 3.82 (3H, s), 3.55 (3H, s), 3.34 (3H, s) ppm. ^{13}C NMR ($CDCl_3$, ppm): δ 169.1, 161.3, 130.2, 125.8, 113.0, 60.6, 55.0, 33.6 ppm.

HRMS (p-ESI) calcd for $C_{10}H_{13}NO_3$+Na $[M+Na]^+$ 218.0788, found 218.0785.

Synthesis of para-L:[45] LDA (22.0 ml, 1.00 M in *n*-hexane and THF, 32.0 mmol) was added dropwise to the solution of 2,5-dimethylpyrazine (1.7ml, 15.5 mmol) in THF (100 ml) at –78 °C under N_2 atmosphere. The reaction mixture was stirred at –78 °C for 1 h, and then **1a** (7.25 g, 34.8 mmol) in THF (50 ml) was added to the solution at –78 °C. After stirred at –78 °C for 1 h, it was warmed to room temperature and continued stirring for 12 h. The reaction solvent was evaporated, then water (100 ml) was added and extracted by DCM (4 × 50 ml). The organic layer was dried over anhydrous sodium sulfate, and the solvent was removed by a rotary evaporator. The residue was purified by reprecipitation (into methanol). After filtration, **para-L** was obtained as orange solid (0.48 g, 10% yield).

^{1}H NMR ($CDCl_3$, ppm): δ 8.57 (keto–keto, s. 2H), 8.43 (keto–enol), 8.34 (keto–enol), 8.24 (enol–enol), 8.06 (m), 7.84 (m), 7.60 (m), 7.50 (m), 7.43 (m), 6.16 (enol-enol), 6.15 (keto-enol), 4.53 (keto–keto, s, 4H), 4.51 (keto–enol) ppm. ^{13}C NMR ($CDCl_3$, ppm, enol-enol): δ 196.0, 163.9, 149.0, 145.0, 133.7, 128.7, 92.1, 45.1 ppm.

HRMS (p-ESI) calcd for $C_{20}H_{16}N_2O_2$+Na $[M+Na]^+$ 339.1104, found. 339.1105.

Synthesis of para-LMeO:[45] LDA (22.0 ml, 1.00 M in *n*-hexane and THF, 22.0 mmol) was added

dropwise to the solution of 2,5-dimethylpyrazine (1.1ml, 10.1 mmol) in THF (50 ml) at –78 °C under N_2 atmosphere. The reaction mixture was stirred at –78 °C for 1 h, and then **1b** (3.30 g, 20.6 mmol) in THF (50 ml) was added to the solution at –78 °C. After stirred at –78 °C for 1 h, it was warmed to room temperature and continued stirring for 12 h. The reaction solvent was evaporated, then water (100 ml) was added and extracted by DCM (4 × 50 ml). The organic layer was dried over anhydrous sodium sulfate, and the solvent was removed by a rotary evaporator. The residue was purified by reprecipitation (into methanol). After filtration, **para-LMeO** was obtained as pale-yellow solid (1.2 g, 32% yield).

^{1}H NMR ($CDCl_3$, ppm): δ 8.55 (2H, s), 8.38 (m), 8.29 (m), 8.04 (4H, m), 6.95 (4H, m), 6.04 (s), 4.46 (4H, s), 4.43 (s), 3.88 (6H, s), 3.86 (s) ppm. ^{13}C NMR ($CDCl_3$, ppm): δ 194.3, 163.9, 149.1, 144.9, 131.0, 129.3, 113.9, 55.5, 44.9 ppm.

HRMS (p-ESI) calcd for $C_{22}H_{20}N_2O_4$+Na $[M+Na]^+$ 399.1315, found 399.1322.

Synthesis of para-B: To a heat-gun-dried round-bottom flask, were added **para-L** (0.324 g, 1.0 mmol) and dimesitylfluoroborane (1.11 g, 4.1 mmol), then toluene (10 ml). To the solution, were added NEt_3 (0.56 ml, 4.0 mmol) under N_2 atmosphere and the reaction mixture was heated (80 °C) for 3 h. The mixture was allowed to cool down, and the solvent was removed under vacuum. The crude product was purified by flash column chromatography on silica gel (DCM/*n*-hexane = 1/1 (v/v), R_f = 0.75) and reprecipitation (DCM into *n*-hexane) to afford **para-B** as a blue solid (34.8 mg, 4% isolated yield).

^{1}H NMR: δ=7.78 (4H, *J* = 7.1 Hz, d), 7.68 (2H, s), 7.35 (6H, m), 6.71 (8H, s), 6.23 (2H, s), 2.22 (12H, s), 2.00 (24H, s) ppm. ^{13}C NMR: δ 166.2, 144.2, 141.9, 138.1, 136.0, 134.3, 130.9, 130.1, 128.4, 126.3, 92.9, 23.8, 20.8 ppm (A peak of the carbon atom adjacent to the boron atom were

not able to be observed due to quadrupolar coupling.). ^{11}B NMR: δ 7.9 ppm.

HRMS (p-ESI) calcd for $C_{56}H_{58}B_2N_2O_2$+Na $[M+Na]^+$ 835.4577, found 835.4595.

Synthesis of para-BMeO: To a heat-gun-dried round-bottom flask, were added **para-LMeO** (0.312 g, 0.83 mmol) and Mes_2BF (1.11 g, 4.14 mmol), then toluene (10 ml). In the solution, were added NEt_3 (0.44 ml, 3.2 mmol) under N_2 atmosphere and the reaction mixture was heated (80 °C) for 3 h. The mixture was allowed to cool down, and the solvent was removed under vacuum. The crude product was purified by flash column chromatography on silica gel (eluent: DCM/*n*-hexane = 1/2 (v/v), R_f = 0.25) and reprecipitation (into *n*-hexane) to afford **para-BMeO** as a green solid (26.6 mg, 4% isolated yield).

^{1}H NMR: δ = 7.73 (4H, J = 9.0 Hz, d), 7.60 (2H, s), 6.83 (4H, J = 9.0 Hz, d), 6.70 (8H, s), 6.11 (2H, s), 3.81 (6H, s), 2.22 (12H, s), 2.00 (24H, s) ppm. ^{13}C NMR: δ= 165.7, 161.9, 143.9, 141.9, 137.9, 135.8, 130.1, 128.1, 126.9, 113.8, 91.6, 23.8, 20.8 ppm (A peak of the carbon atom adjacent to the boron atom were not able to be observed due to quadrupolar coupling.). ^{11}B NMR: δ= 6.67 ppm.

HRMS (p-ESI) calcd for $C_{58}H_{62}B_2N_2O_4$+Na $[M+Na]^+$ 865.4788, found 895.4794.

Synthesis of ortho-L: LDA (30.0 ml, 1.00 M in *n*-hexane and THF, 30.0 mmol) was added dropwise to the solution of 2,3-dimethylpyrazine (1.6 ml, 15.0 mmol) in THF (100 ml) at –78 °C under N_2 atmosphere. The reaction mixture was stirred at –78 °C for 1 h, and then *N*-methoxy-*N*-methylbenzamide (6.29 g, 38.1 mmol) in THF (50 ml) was added to the solution at –78 °C. After stirred at –78 °C for 1 h, it was warmed to room temperature and continued stirring for 12 h. The reaction solvent was evaporated, then water (100 ml) was added and extracted with CH_2Cl_2 (4 ×

50 ml). The organic layer was dried over anhydrous sodium sulfate, and the solvent was removed by a rotary evaporator. The residue was purified by column chromatography on silica gel (eluent: CH_2Cl_2/EtOAc = 14/1 (v/v), R_f = 0.23). Then, methanol was added into the resulting brown oil and left at room temperature until crystallization. After filtration, **ortho-L** was obtained as an orange crystal (0.38 g, 8% yield).

^{1}H NMR ($CDCl_3$, ppm): δ 8.24 (*J* = 2.6 Hz, d), 8.18 (*J* = 3.0 Hz, d), 8.10 (*J* = 7.5 Hz, d), 7.89–7.93 (m), 7.77–7.80 (m), 7.58–7.61 (m), 7.45–7.51 (m), 7.39–7.40 (m), 6.36 (s, enol–enol), 6.19 (s, keto–enol), 4.62 (s, keto–enol), –4.84 (s), –5.39 (s)

^{13}C NMR of the ***ortho*-L** was not fully characterized due to the complicated tautomerizations (Figure S3).

HRMS (p-ESI) calcd for $C_{20}H_{16}N_2O_2$+Na $[M+Na]^+$ 339.1104, found. 339.1111.

Synthesis of ortho-B: To a heat-gun-dried round-bottom flask, were added **ortho-L** (0.32 g, 1.0 mmol) and dimesitylfluoroborane (1.09 g, 4.0 mmol), then toluene (10 ml). To the solution, were added NEt_3 (0.56 ml, 4.0 mmol) under N_2 atmosphere and the reaction mixture was heated at 80 °C for 3 h. The mixture was allowed to cool down, and the solvent was removed under vacuum. The crude product was purified by flash column chromatography on silica gel (CH_2Cl_2/*n*-hexane = 1/1 (v/v), R_f = 0.63) to afford a red solid after evaporation. The resulting solid was filtered and washed with *n*-hexane, then **ortho-B** was obtained as a red cocrystal containing CH_2Cl_2 and *n*-hexane (95.8 mg, 15% yield).

^{1}H NMR ($CDCl_3$, ppm): δ 7.95 (4H, *J* = 7.1 Hz, d), 7.48–7.52 (2H, m), 7.41–7.45 (4H, m), 7.13 (2H, s), 6.68 (8H, s), 6.64 (2H, s), 2.19 (12H, s), 1.98 (24H, s) ppm.

^{13}C{^{1}H} NMR ($CDCl_3$, ppm): δ 172.9, 147.3, 141.9, 135.8, 133.9, 132.3, 130.0, 129.2, 128.7,

127.3, 90.4, 23.9, 20.8 ppm (A peak of the carbon atoms adjacent to the boron atoms were not able to be observed due to quadrupolar coupling.).

$^{11}B\{^{1}H\}$ NMR ($CDCl_3$, ppm): δ 7.26 ppm.

HRMS (n-ESI) calcd for $C_{56}H_{58}B_2N_2O_2$ $[M]^-$ 812.4690, found 812.4715.

Photophysical Measurements: UV–vis absorption spectra were recorded on a Shimadzu UV-3600 spectrophotometer. Photoluminescence (PL) spectra were measured with a HORIBA FluoroLog-3 spectrofluorometer, and photoluminescence quantum yields were measured by the integrating sphere method using Hamamatsu Photonics Quantaurus-QY Plus. Fluorescence lifetime analyses were carried out on a HORIBA FluoroCube spectrofluorometer system; excitation at 375 nm using a UV diode laser (NanoLED-375L).

Acknowledgements

Computation time was provided by the SuperComputer System, Institute for Chemical Research, Kyoto University. This work was partially supported by the Kato Foundation for Promotion of Science (for K.T.) and Grant-in-Aid for Early-Career Scientists (for S.I., JSPS KAKENHI Grant Numbers 21K14673 and 23K13793), for Scientific Research (B) (for K.T., JSPS KAKENHI Grant Number, 21H02001), and for Exploratory Research (for K.T., JSPS KAKENHI Grant numbers 21K19002), and a Grant-in-Aid of The Ministry of Education, Culture, Sports, Science, and Technology, Japan, for Scientific Research on Innovative Areas “New Polymeric Materials Based on Element-Blocks (No. 2401)” (JP24102013).

Conflicts of Interest

The authors declare no conflict of interest.

Keywords: Boron; Pyrazine; Fluorescence; Near-infrared emission; Aggregation-induced emission enhancement

References

[1] S.-Y. Chang, P. Cheng, G. Li, Y. Yang, *Joule* **2018**, *2*, 1039–1054.

[2] J. Fabian, H. Nakazumi, M. Matsuoka, *Chem. Rev.* **1992**, *92*, 1197–1226.

[3] Y.-J. Cheng, S.-H. Yang, C.-S. Hsu, *Chem. Rev.* **2009**, *109*, 5868–5923.

[4] P. Cheng, G. Li, X. Zhan, Y. Yang, *Nat. Photonics* **2018**, *12*, 131–142.

[5] A. Zampetti, A. Minotto, F. Cacialli, *Adv. Funct. Mater.* **2019**, *29*, 1905825.

[6] Z. Cheng, Y. Wu, Z. Xiong, S. S. Gambhir, X. Chen, *Bioconjugate Chem.* **2005**, *16*, 1433–1441.

[7] V. J. Pansare, S. Hejazi, W. J. Faenza, R. K. Prud'homme, *Chem. Mater.* **2012**, *24*, 812–827.

[8] R. Weinstain, T. Slanina, D. Kand, P. Klán, *Chem. Rev.* **2020**, *120*, 13135–13272.

[9] W. Sun, S. Guo, C. Hu, J. Fan, X. Peng, *Chem. Rev.* **2016**, *116*, 7768–7817.

[10] L. Yuan, W. Lin, Y. Yang, H. Chen, *J. Am. Chem. Soc.* **2012**, *134*, 1200–1211.

[11] A. C. Sedgwick, L. Wu, H.-H. Han, S. D. Bull, X.-P. He, T. D. James, J. L. Sessler, B. Z. Tang, H. Tian, J. Yoon, *Chem. Soc. Rev.* **2018**, *47*, 8842–8880.

[12] A. Tsuda, A. Osuka, *Science* **2001**, *293*, 79–82.

[13] M. Adachi, Y. Nagao, *Chem. Mater.* **2001**, *13*, 662–669.

[14] A. Wadsworth, M. Moser, A. Marks, M. S. Little, N. Gasparini, C. J. Brabec, D. Baran, I. McCulloch, *Chem. Soc. Rev.* **2018**, *48*, 1596–1625.

[15] Q. Miao, *Adv. Mater.* **2014**, *26*, 5541–5549.

[16] G. Long, X. Yang, W. Chen, M. Zhang, Y. Zhao, Y. Chen, Q. Zhang, *Phys. Chem. Chem. Phys.* **2015**, *18*, 3173–3178.

[17] M. J. G. Lesley, A. Woodward, N. J. Taylor, T. B. Marder, I. Cazenobe, I. Ledoux, J. Zyss, A. Thornton, D. W. Bruce, A. K. Kakkar, *Chem. Mater.* **1998**, *10*, 1355–1365.

[18] A. G. Crawford, A. D. Dwyer, Z. Liu, A. Steffen, A. Beeby, L.-O. Pålsson, D. J. Tozer, T. B. Marder, *J. Am. Chem. Soc.* **2011**, *133*, 13349–13362.

[19] A. G. Crawford, Z. Liu, I. A. I. Mkhalid, M. Thibault, N. Schwarz, G. Alcaraz, A. Steffen, J. C. Collings, A. S. Batsanov, J. A. K. Howard, T. B. Marder, *Chem. Eur. J.* **2012**, *18*, 5022–5035.

[20] L. Ji, R. M. Edkins, A. Lorbach, I. Krummenacher, C. Brückner, A. Eichhorn, H. Braunschweig, B. Engels, P. J. Low, T. B. Marder, *J. Am. Chem. Soc.* **2015**, *137*, 6750–6753.

[21] J. Merz, J. Fink, A. Friedrich, I. Krummenacher, H. H. Al Mamari, S. Lorenzen, M. Haehnel, A. Eichhorn, M. Moos, M. Holzapfel, H. Braunschweig, C. Lambert, A. Steffen, L. Ji, T. B. Marder, *Chem. Eur. J.* **2017**, *23*, 13164–13180.

[22] J. Merz, M. Dietz, Y. Vonhausen, F. Wöber, A. Friedrich, D. Sieh, I. Krummenacher, H. Braunschweig, M. Moos, M. Holzapfel, C. Lambert, T. B. Marder, *Chem. Eur. J.* **2020**, *26*, 438–453.

[23] G. K. Kole, J. Merz, A. Amar, B. Fontaine, A. Boucekkine, J. Nitsch, S. Lorenzen, A. Friedrich, I. Krummenacher, M. Košćak, H. Braunschweig, I. Piantanida, J. Halet, K. Müller-Buschbaum, T. B. Marder, *Chem. Eur. J.* **2021**, *27*, 2837–2853.

[24] N. Ito, T. Hirose, K. Matsuda, *Org. Lett.* **2014**, *16*, 2502–2505.

[25] H. Kubo, T. Hirose, K. Matsuda, *Org. Lett.* **2017**, *19*, 1776–1779.

[26] X. Jia, J. Nitsch, L. Ji, Z. Wu, A. Friedrich, F. Kerner, M. Moos, C. Lambert, T. B. Marder, *Chem. Eur. J.* **2019**, *25*, 10845–10857.

[27] J. K. G. Karlsson, A. Harriman, *J. Phys. Chem.* **2016**, *120*, 2537–2546.

[28] H. Watanabe, M. Hirose, K. Tanaka, Y. Chujo, *Chem. Commun.* **2017**, *53*, 5036–5039.

[29] H. Watanabe, Y. Kawano, K. Tanaka, Y. Chujo, *Asian J. Org. Chem.* **2020**, *9*, 259–266.

[30] K. Tanaka, Y. Chujo, *Chem. Lett.* **2021**, *50*, 269–279.

[31] H. Watanabe, K. Tanaka, Y. Chujo, *J. Org. Chem.* **2019**, *84*, 2768–2778.

[32] H. Watanabe, J. Ochi, K. Tanaka, Y. Chujo, *Eur J. Org. Chem.* **2020**, *2020*, 777–783.

[33] A. Wakamiya, T. Taniguchi, S. Yamaguchi, *Angew. Chem. Int. Ed.* **2006**, *45*, 3170–3173.

[34] C. Zeng, K. Yuan, N. Wang, T. Peng, G. Wu, S. Wang, *Chem. Sci.* **2018**, *10*, 1724–1734.

[35] C. Zhu, Z.-H. Guo, A. U. Mu, Y. Liu, S. E. Wheeler, L. Fang, *J. Org. Chem.* **2016**, *81*, 4347–4352.

[36] S. Oda, T. Shimizu, T. Katayama, H. Yoshikawa, T. Hatakeyama, *Org. Lett.* **2019**, *21*, 1770–1773.

[37] X. Peng, F. Song, E. Lu, Y. Wang, W. Zhou, J. Fan, Y. Gao, *J. Am. Chem. Soc.* **2005**, *127*, 4170–4171.

[37] Y. Yu, J. Wang, H. Xiang, L. Ying, C. Wu, H. Zhou, H. Liu, *Dyes Pigm.* **2020**, *183*, 108710.

[39] K. Suenaga, K. Tanaka, Y. Chujo, *Eur J. Org. Chem.* **2017**, *2017*, 5191–5196.

[40] M. Yamaji, S. Kato, K. Tomonari, M. Mamiya, K. Goto, H. Okamoto, Y. Nakamura, F. Tani, *Inorg. Chem.* **2017**, *56*, 12514–12519.

[41] G. Tan, I. Maisuls, F. Strieth-Kalthoff, X. Zhang, C. Daniliuc, C. A. Strassert, F. Glorius, *Adv. Sci.* **2021**, *8*, 2101814.

[42] C. M. Cardona, W. Li, A. E. Kaifer, D. Stockdale, G. C. Bazan, *Adv. Mater.* **2011**, *23*, 2367–2371.

[43] M. J. Frisch, G. W. Trucks, H. B. Schlegel, G. E. Scuseria, M. A. Robb, J. R. Cheeseman, G. Scalmani, V. Barone, G. A. Petersson, H. Nakatsuji, X. Li, M. Caricato, A. V. Marenich, J. Bloino, B. G. Janesko, R. Gomperts, B. Mennucci, H. P. Hratchian, J. V. Ortiz, A. F. Izmaylov, J. L. Sonnenberg, D. Williams-Young, F. Ding, F. Lipparini, F. Egidi, J. Goings, B. Peng, A. Petrone, T. Henderson, D. Ranasinghe, V. G. Zakrzewski, J. Gao, N. Rega, G. Zheng, W. Liang, M. Hada, M. Ehara, K. Toyota, R. Fukuda, J. Hasegawa, M. Ishida, T. Nakajima, Y. Honda, O. Kitao, H. Nakai, T. Vreven, K. Throssell, J. A. Montgomery, Jr., J. E. Peralta, F. Ogliaro, M. J. Bearpark, J. J. Heyd, E. N. Brothers, K. N. Kudin, V. N. Staroverov, T. A. Keith, R. Kobayashi, J. Normand, K. Raghavachari, A. P. Rendell, J. C. Burant, S. S. Iyengar, J. Tomasi, M. Cossi, J. M. Millam, M. Klene, C. Adamo, R. Cammi, J. W. Ochterski, R. L. Martin, K. Morokuma, O. Farkas, J. B. Foresman, D. J. Fox, *Gaussian 16 Rev. C.01*, Wallingford, CT, **2016**.

[44] N. Wang, J. Wang, Y.-L. Guo, L. Li, Y. Sun, Z. Li, H.-X. Zhang, Z. Guo, Z.-L. Li, X.-Y. Liu, *Chem. Commun.* **2018**, *54*, 8885–8888.

[45] S. Saotome, K. Suenaga, K. Tanaka, Y. Chujo, *Mater. Chem. Front.* **2020**, *4*, 1781–1788.

TOC Graphic

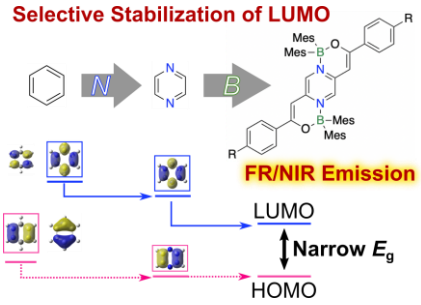

Twitter: @kyotopolymer

Table of Contents

1. Experimental Details

^{1}H (400 MHz) and $^{13}C\{^{1}H\}$ (100 MHz) NMR spectra were recorded on JEOL JNM-AL400 spectrometers. ^{1}H NMR spectra were recorded by using tetramethylsilane (TMS) as an internal standard in $CDCl_3$. ^{13}C NMR spectra were recorded by using residual non-deuterated solvents as an internal standard in $CDCl_3$. $^{11}B\{^{1}H\}$ NMR spectra were referenced externally to $BF_3{\cdot}OEt_2$. High-resolution mass spectra (HRMS) were obtained on a Thermo Fisher EXACTIVE for electron spray ionization (ESI). UV–vis absorption spectra were recorded on a Shimadzu UV-3600 spectrophotometer. Photoluminescence (PL) spectra were measured with a HORIBA FluoroLog-3 spectrofluorometer, and photoluminescence quantum yields were calculated by the integrating sphere method using Hamamatsu Photonics Quantaurus-QY Plus. Fluorescence lifetime analyses were carried out on a HORIBA FluoroCube spectrofluorometer system; excitation at 375 nm using a UV diode laser (NanoLED-375L). Cyclic voltammetry (CV) was carried out on a BAS ALS-Electrochemical-Analyzer Model 600D with a glassy carbon micro working electrode, a Pt counter electrode, an Ag/Ag^{+} reference electrode, and the ferrocene/ferrocenium external reference at a scan rate of 0.1 V s^{-1}. All reactions were performed under N_2 atmosphere. TLC analysis was performed on silica gel plates coated with fluorescent indicator (silica gel 60 Merck F254).

2. NMR Spectra

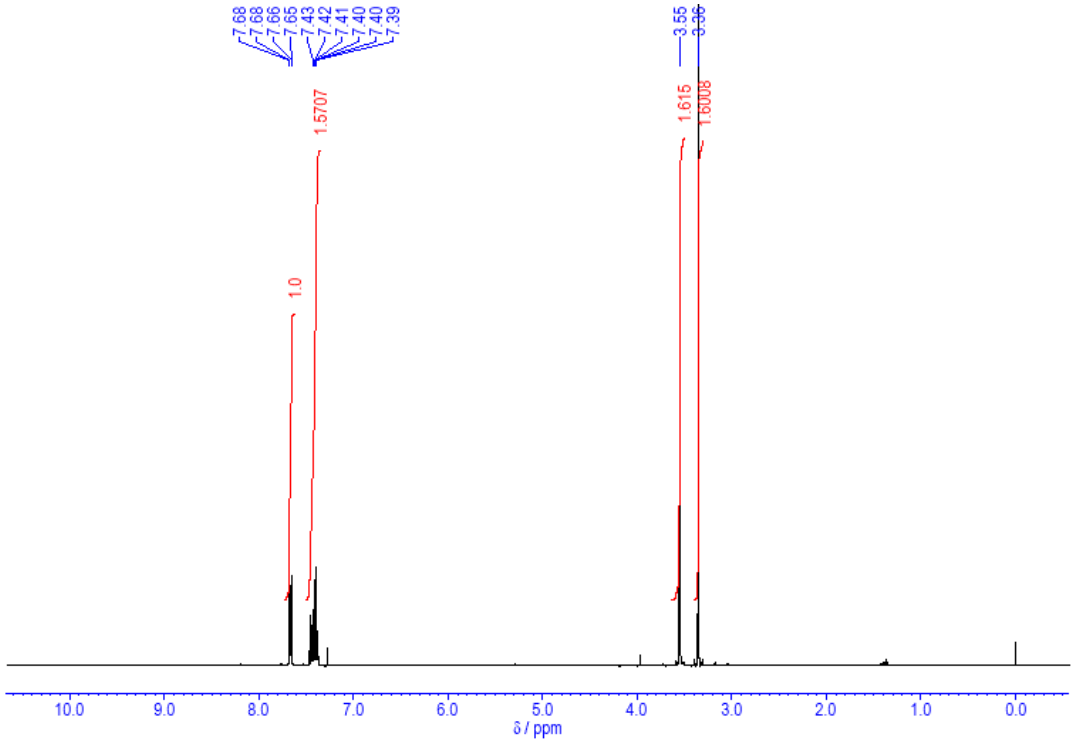

Figure S1. ^{1}H NMR spectrum of **1a** in $CDCl_3$.

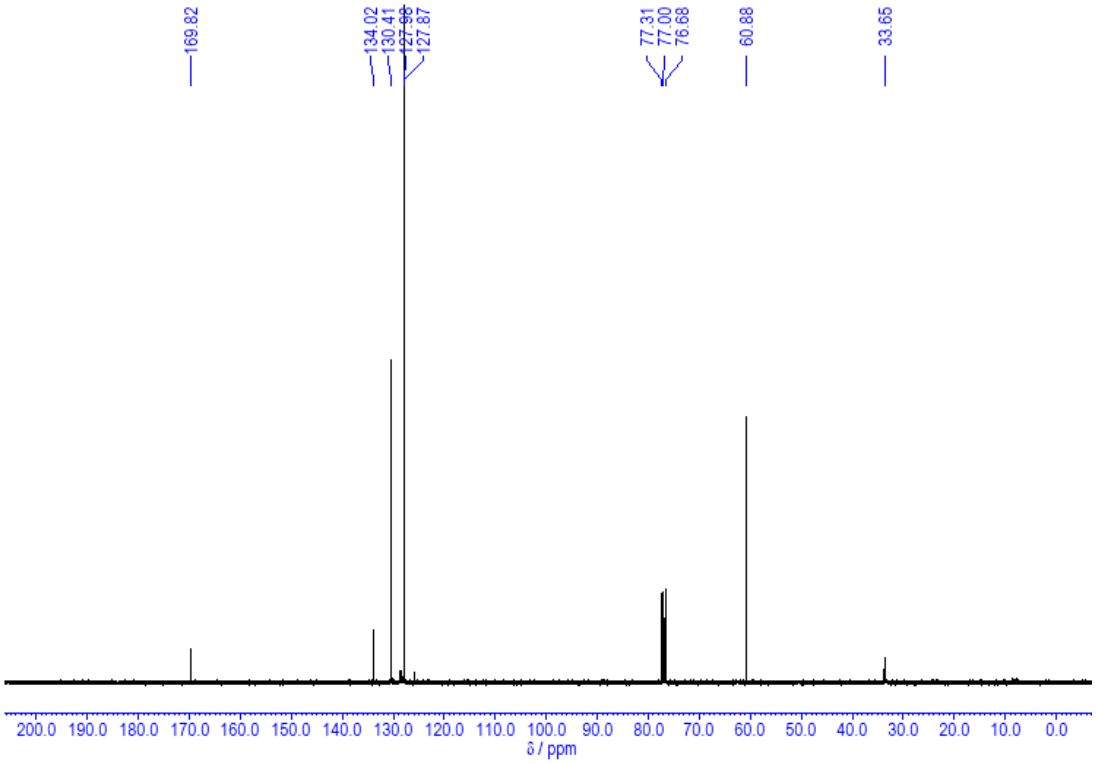

Figure S2. ^{13}C NMR spectrum of **1a** in $CDCl_3$.

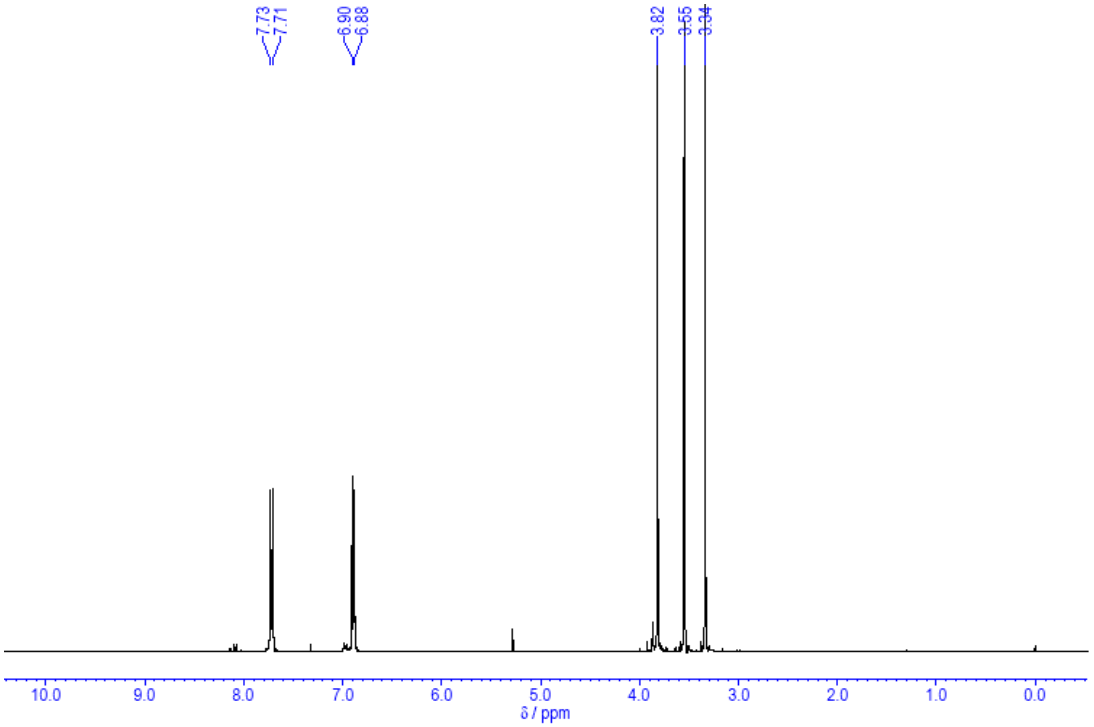

Figure S3. ^{1}H NMR spectrum of **1b** in $CDCl_3$.

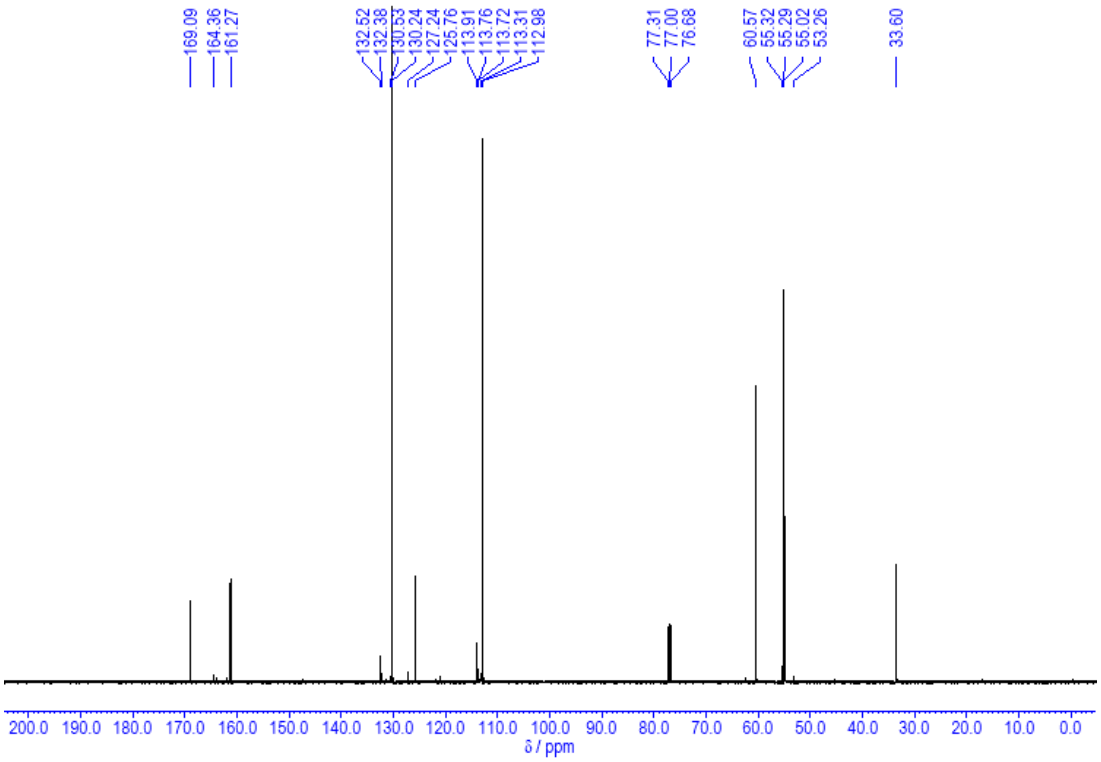

Figure S4. ^{13}C NMR spectrum of **1b** in $CDCl_3$.

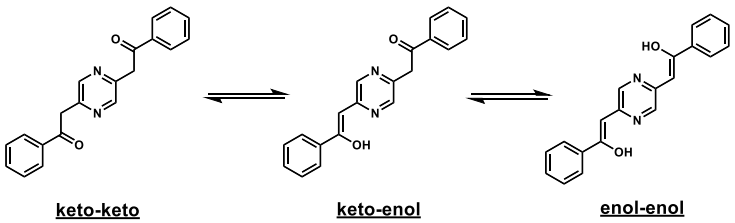

Figure S5. Structures of keto–enol tautomers of **para-L**.

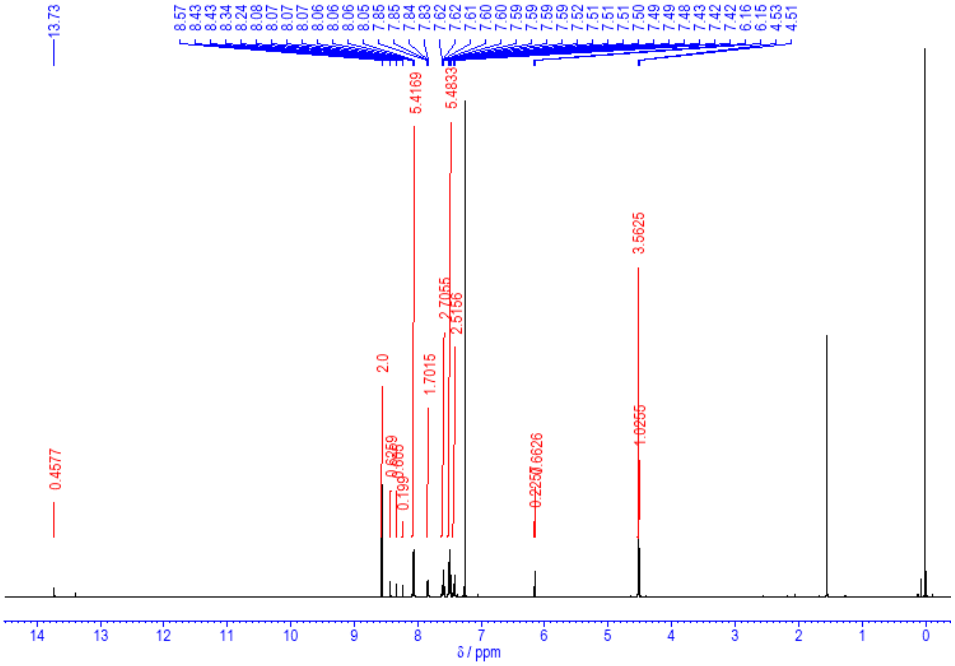

Figure S6. ^{1}H NMR spectrum of **para-L** in $CDCl_3$.

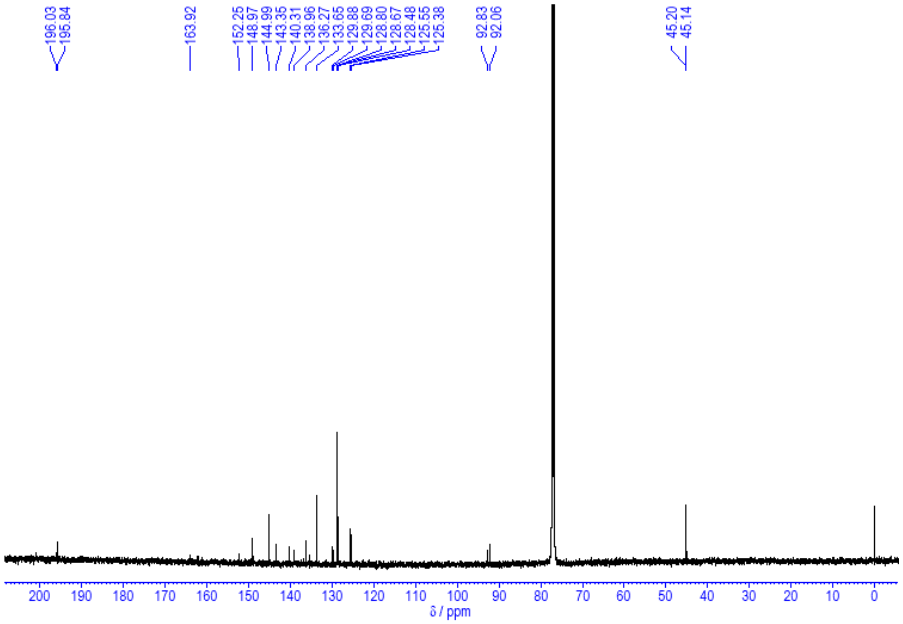

Figure S7. ^{13}C NMR spectrum of **para-L** in $CDCl_3$.

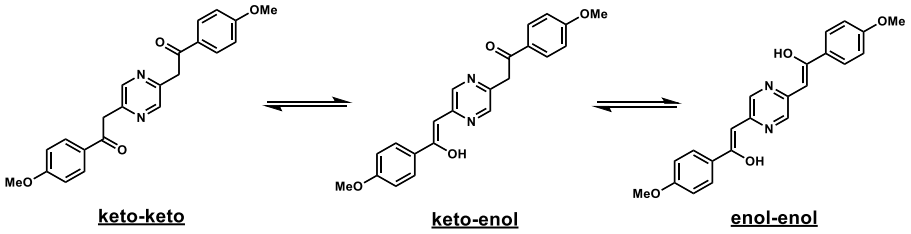

Figure S8. Structures of keto–enol tautomers of **para-LMeO**.

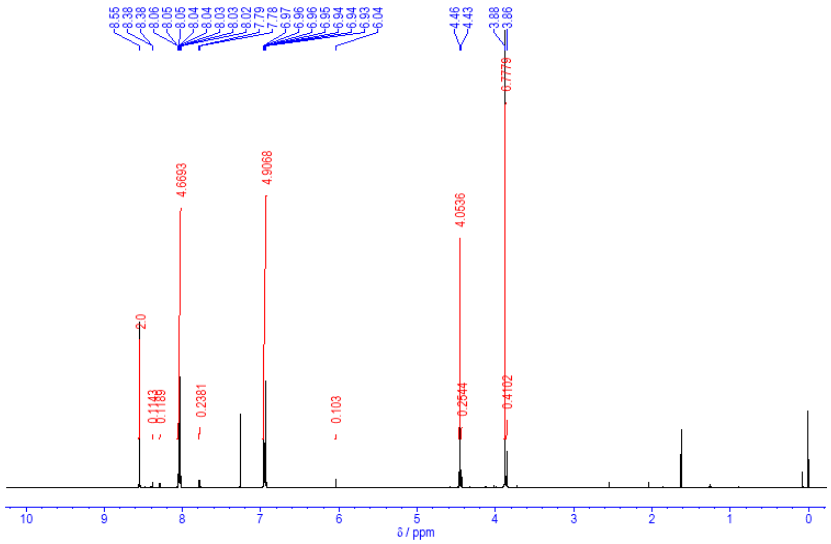

Figure S9. ^{1}H NMR spectrum of **para-LMeO** in $CDCl_3$.

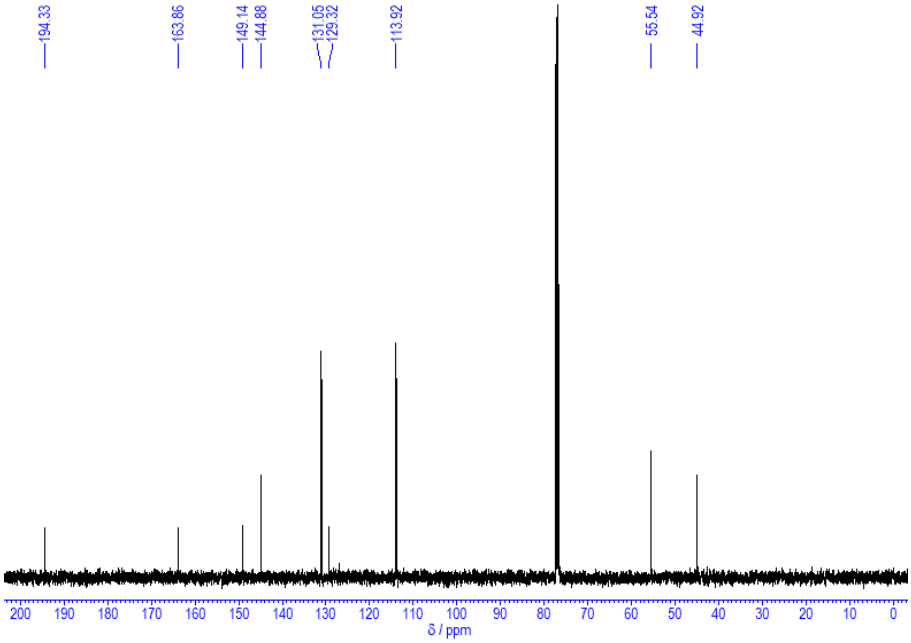

Figure S10. ^{13}C NMR spectrum of **para-LMeO** in $CDCl_3$.

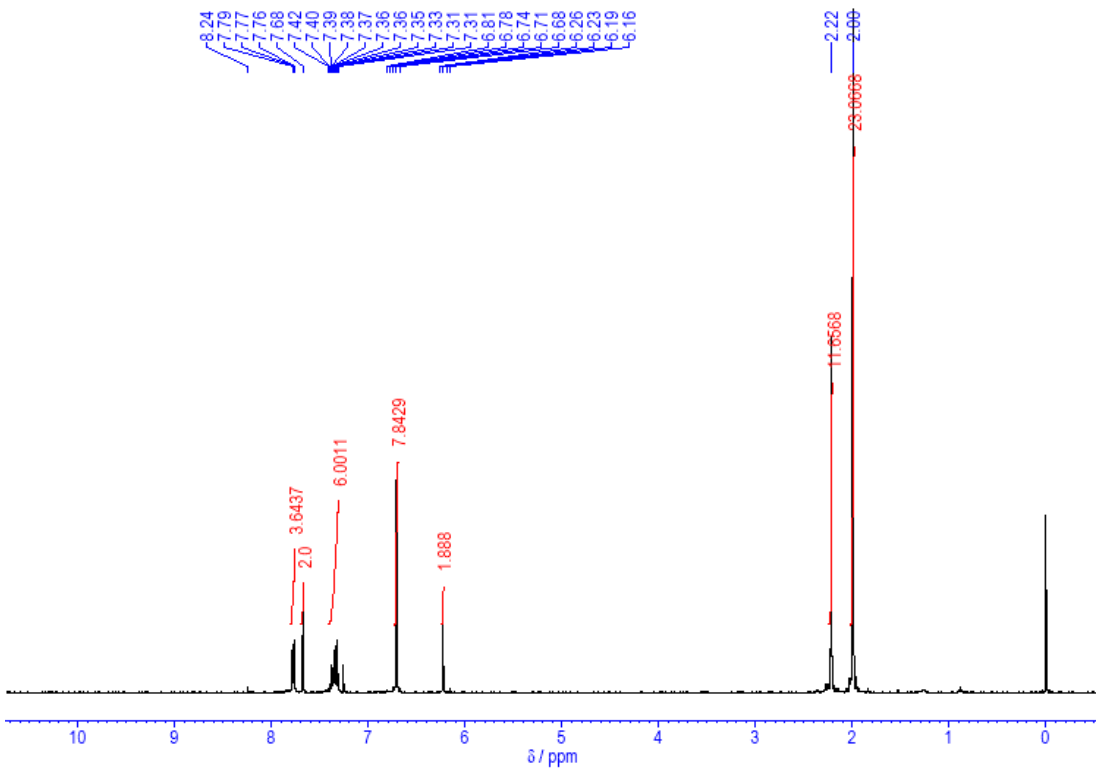

Figure S11. ^{1}H NMR spectrum of **para-B** in $CDCl_3$.

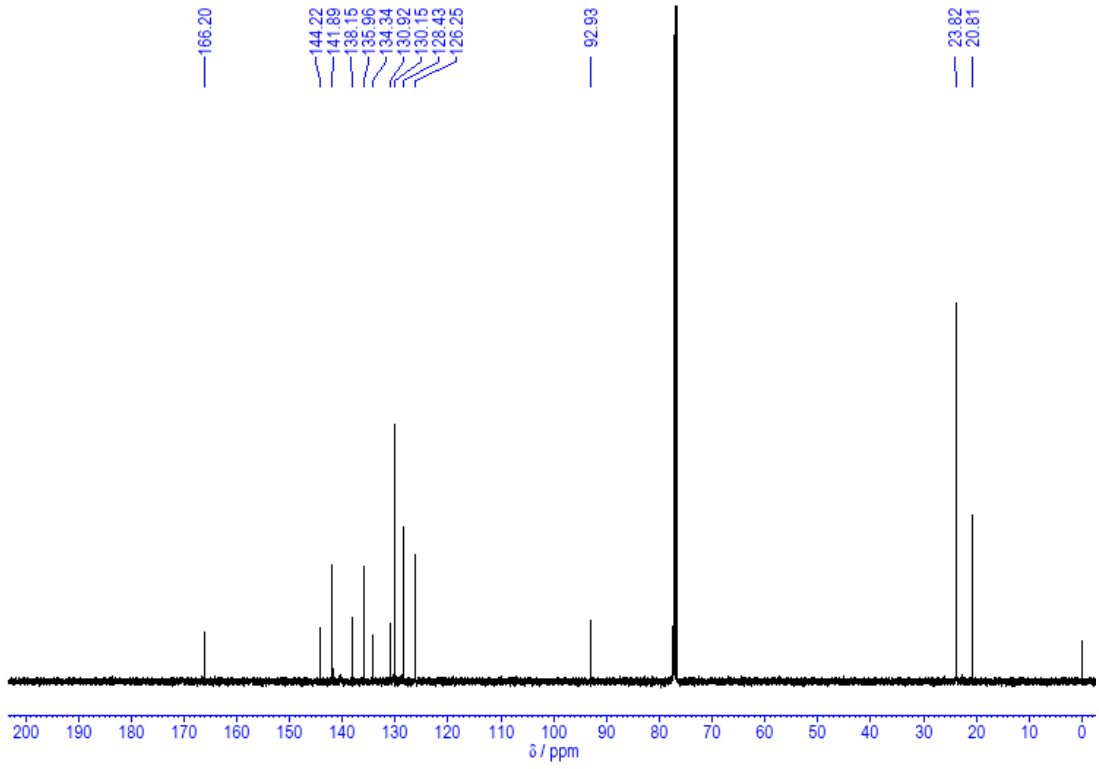

Figure S12. ^{13}C NMR spectrum of **para-B** in $CDCl_3$.

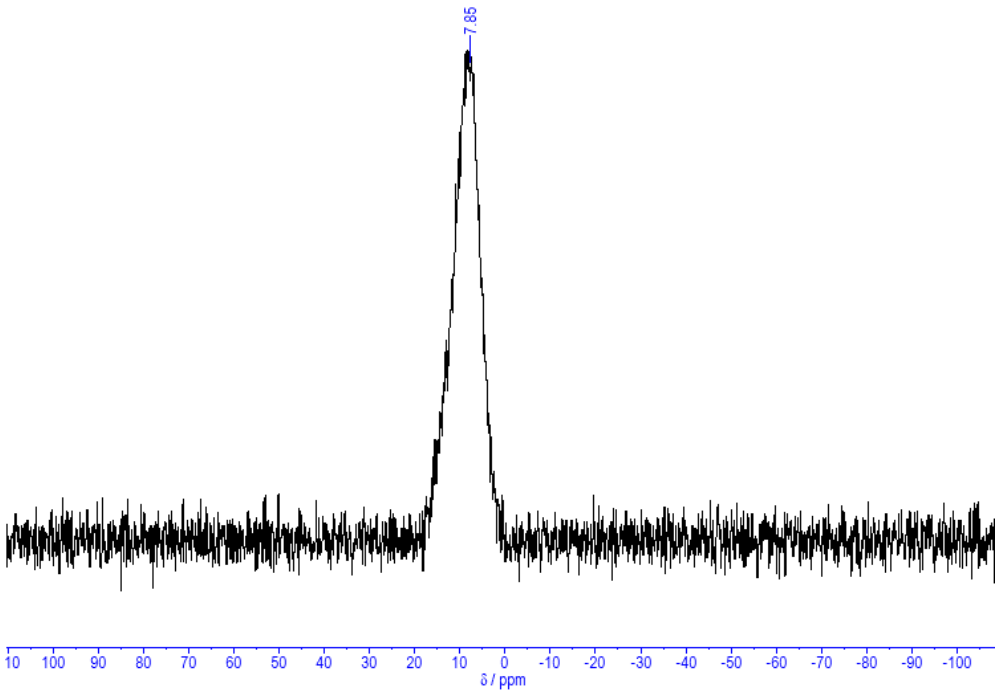

Figure S13. ^{11}B NMR spectrum of **para-B** in $CDCl_3$.

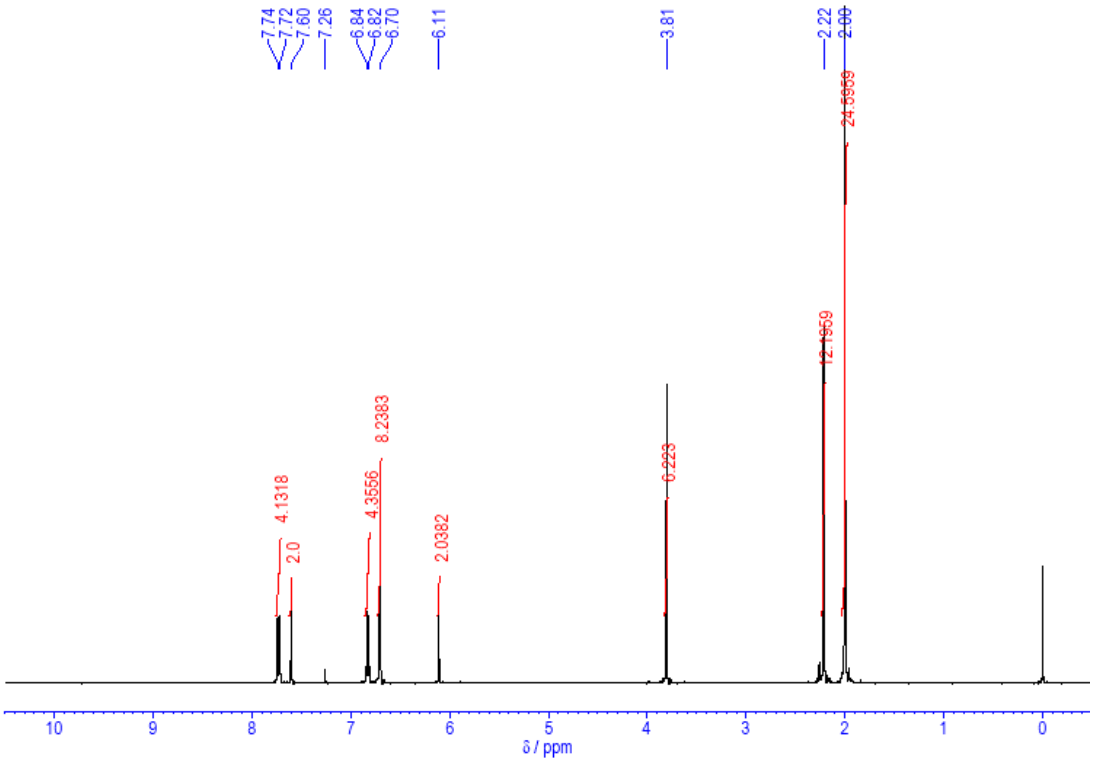

Figure S14. ^{1}H NMR spectrum of **para-BMeO** in $CDCl_3$.

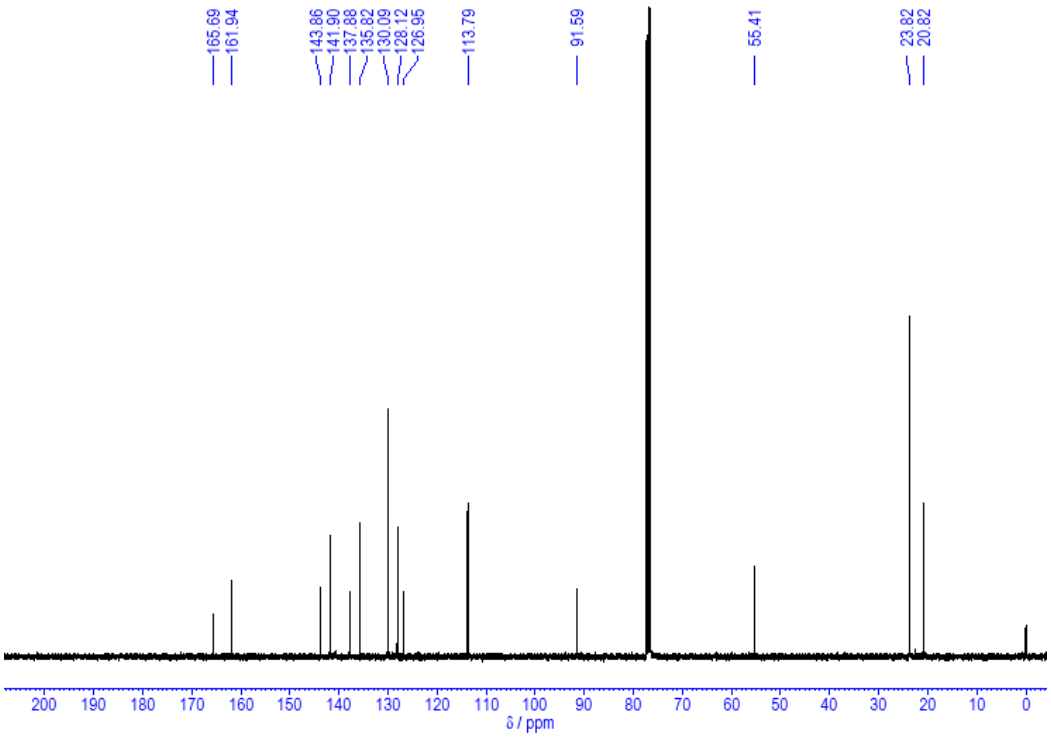

Figure S15. ^{13}C NMR spectrum of **para-BMeO** in $CDCl_3$.

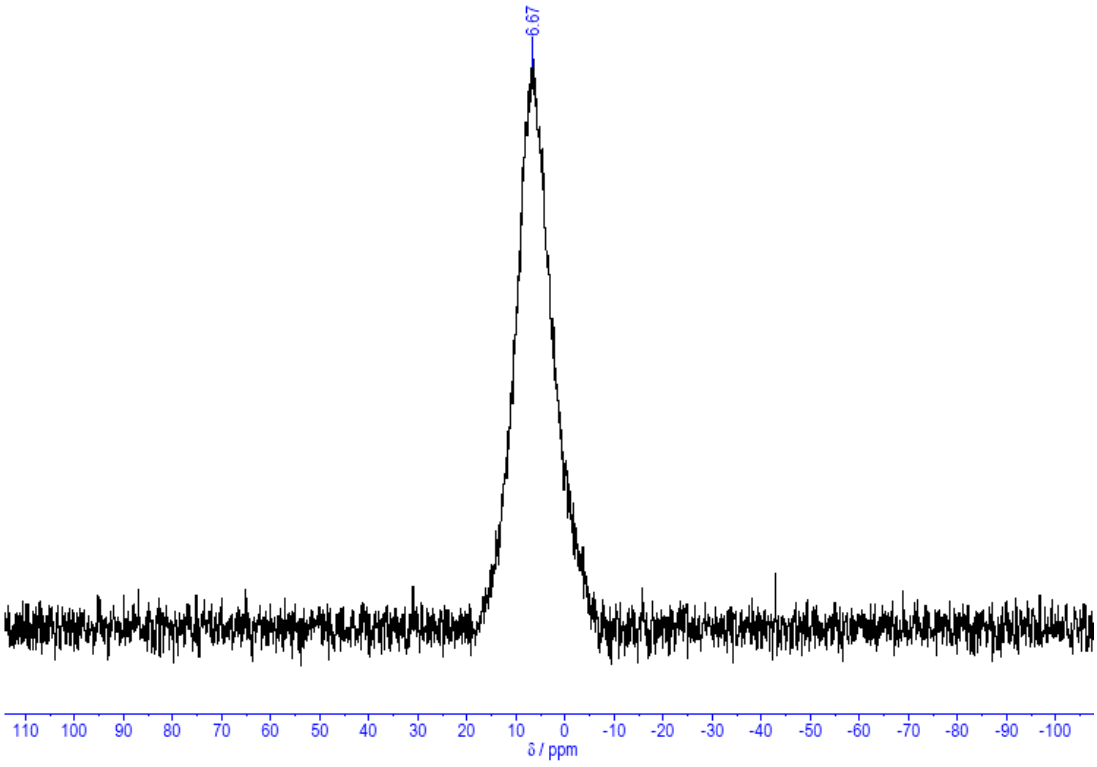

Figure S16. ^{11}B NMR spectrum of **para-BMeO** in $CDCl_3$.

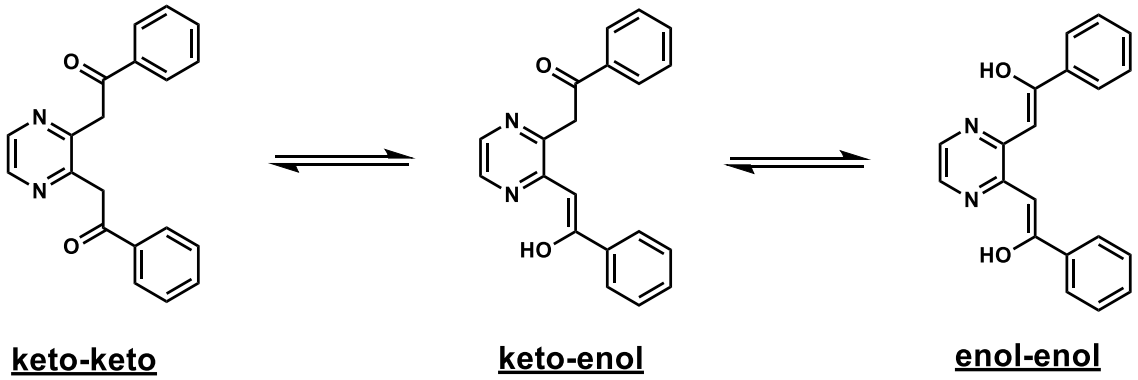

Figure S17. Chemical structures of keto and enol tautomers of **ortho-L.**

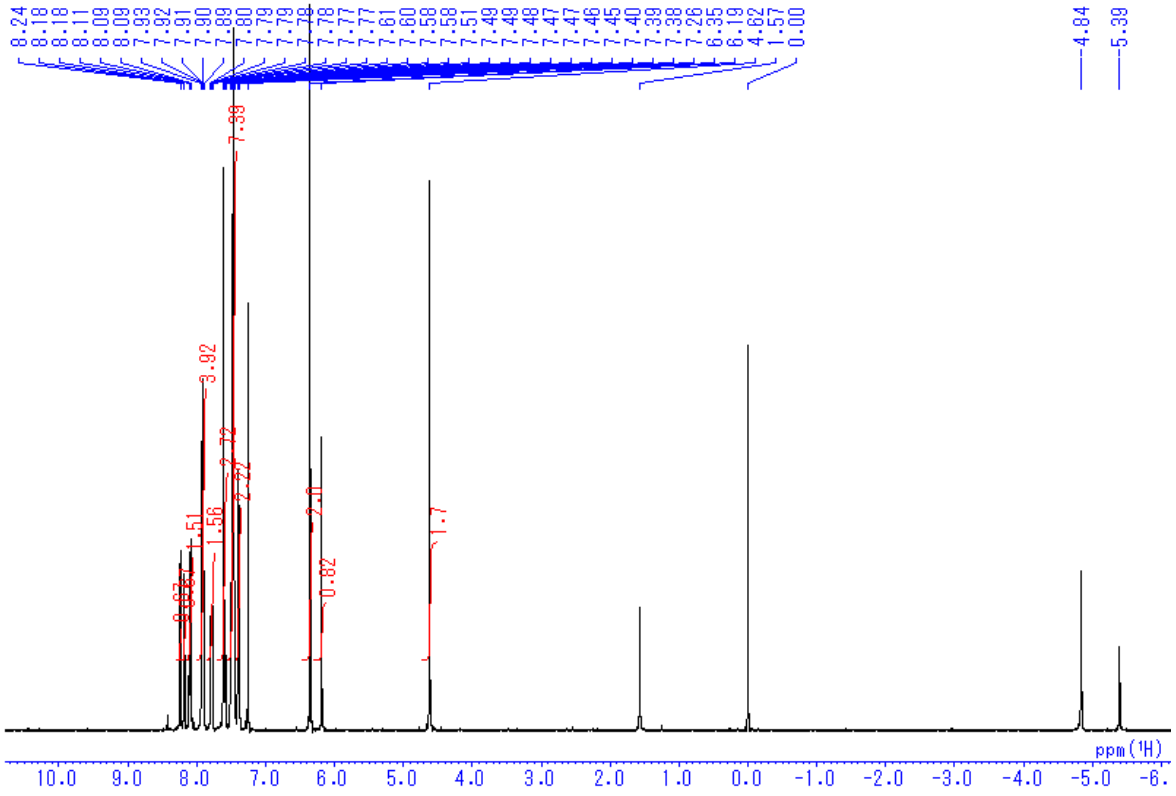

Figure S18. ^{1}H NMR spectrum of **ortho-L** in $CDCl_3$.

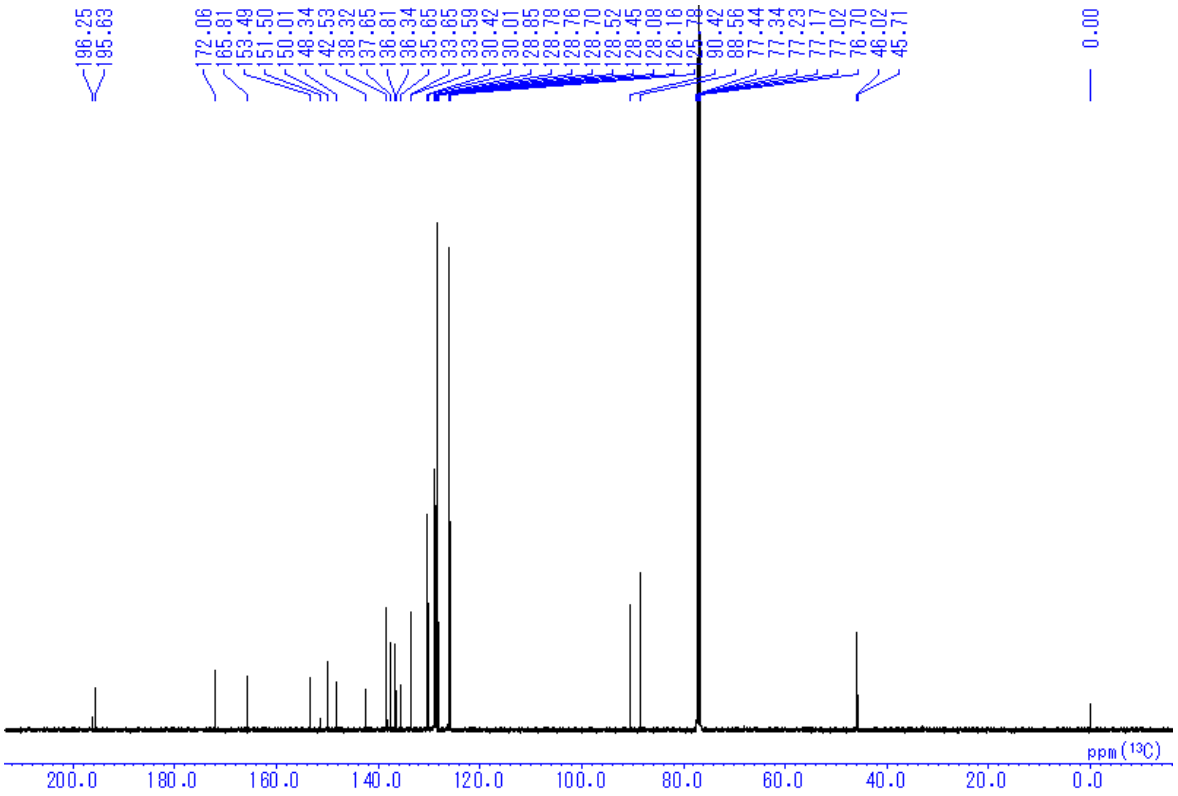

Figure S19. $^{13}C\{^{1}H\}$ NMR spectrum of **ortho-L** in $CDCl_3$.

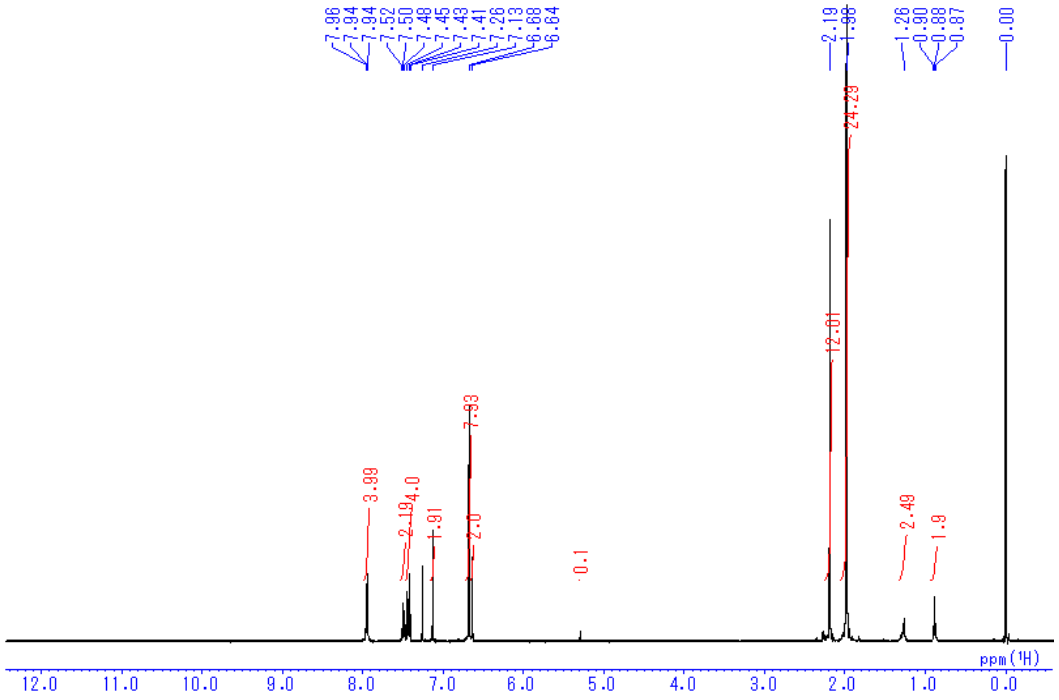

Figure S20. ^{1}H NMR spectrum of **ortho-B** in $CDCl_3$.

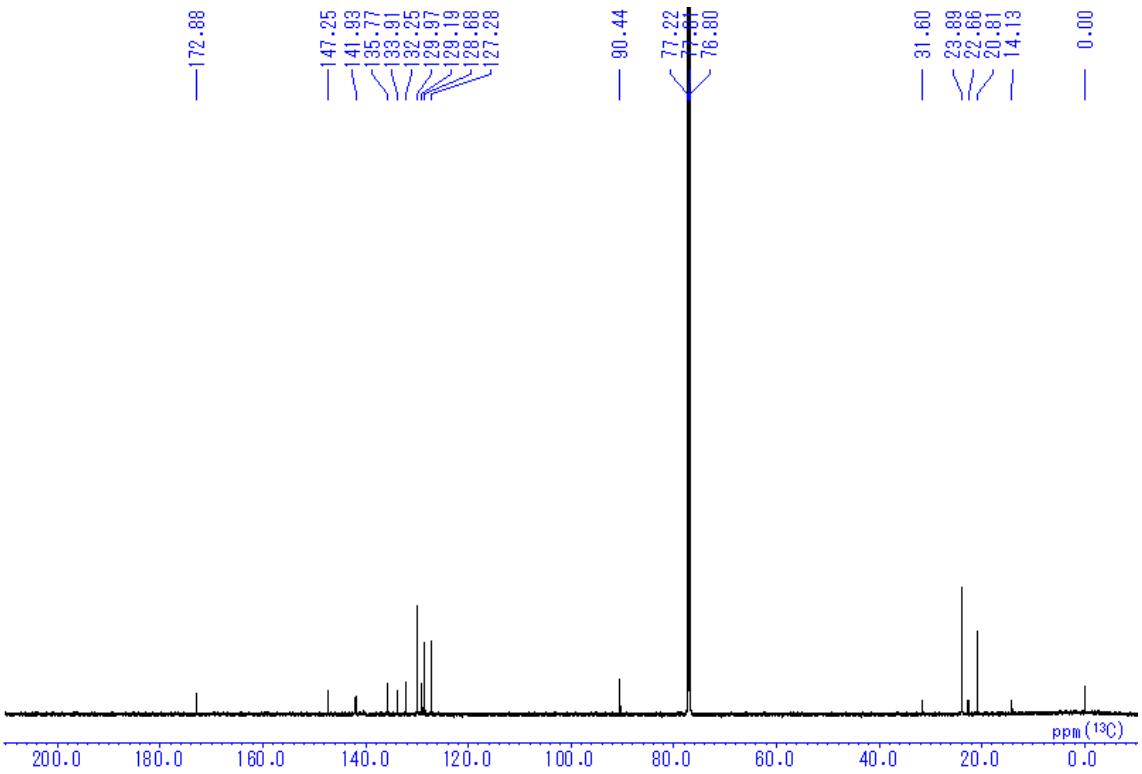

Figure S21. $^{13}C\{^{1}H\}$ NMR spectrum of **ortho-B** in $CDCl_3$.

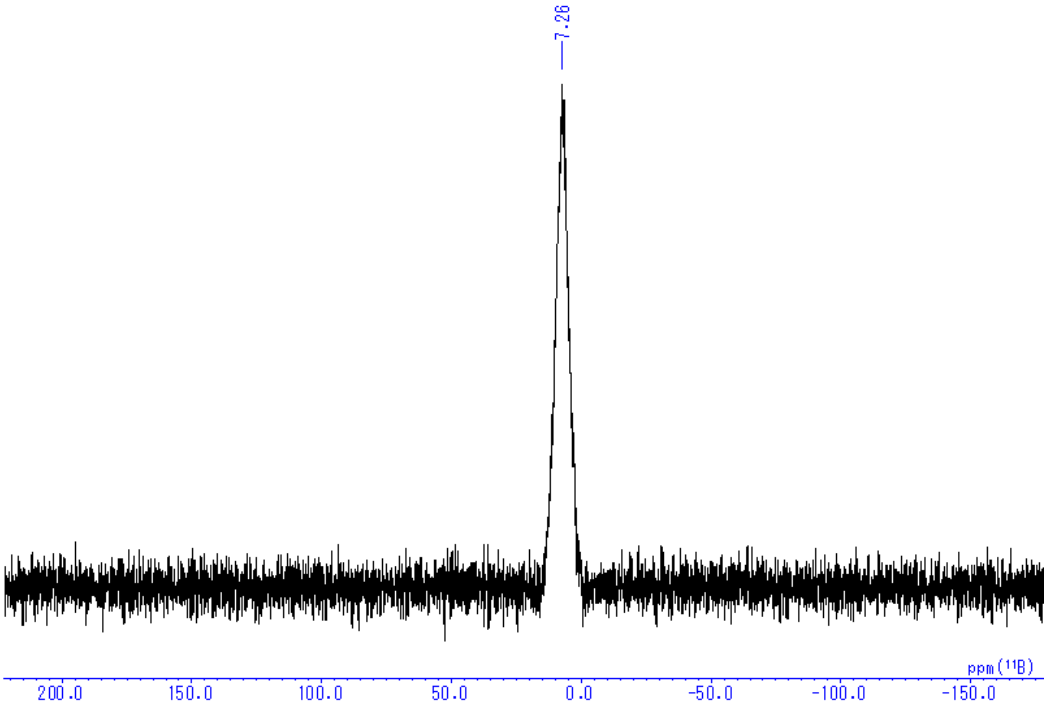

Figure S22. $^{11}B\{^{1}H\}$ NMR spectrum of **ortho-B** in $CDCl_3$.

3. Photophysical and Electrochemical Properties

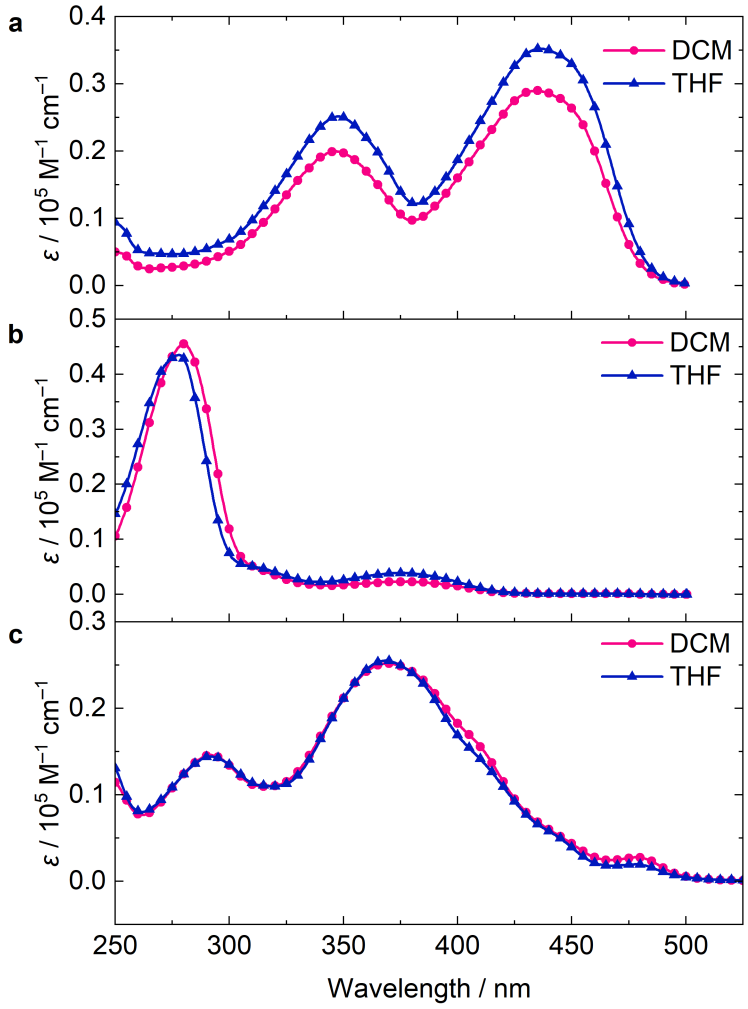

Figure S23. UV–vis absorption spectra of (a) **para-L**, (b) **para-LMeO**, and (c) **ortho-L** in dichloromethane (DCM) and tetrahydrofuran (THF) (1.0×10^{-5} M). Emission was not detected from these ligands.

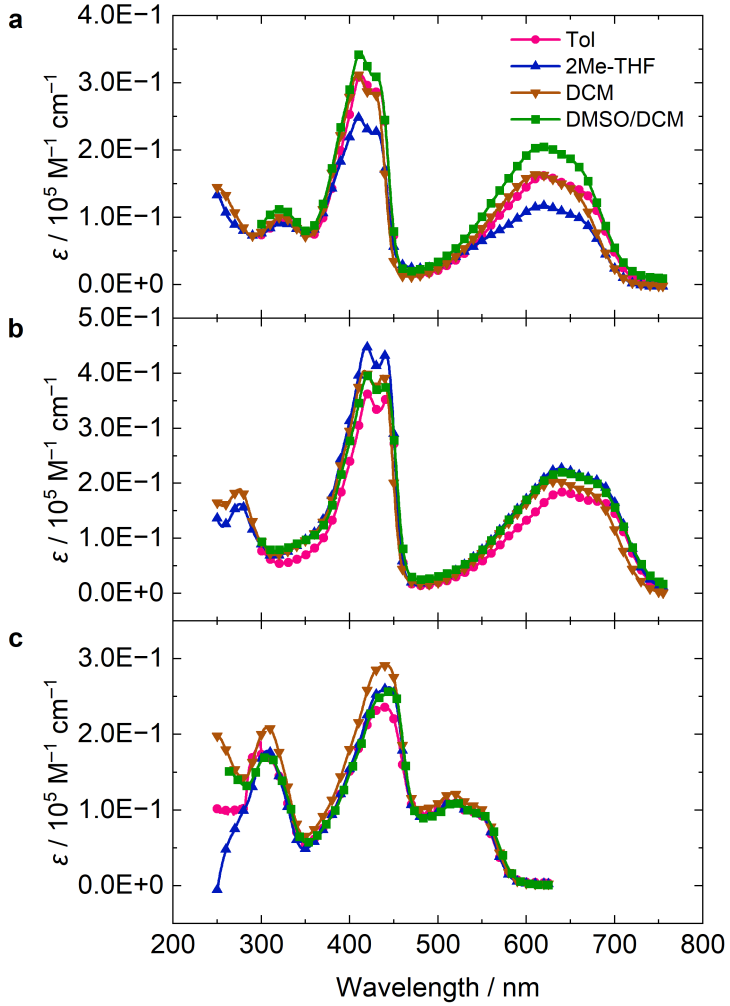

Figure S24. UV–vis–NIR absorption spectra in various solvent (1.0×10^{-5} M for each) of (a) **para-B**, (b) **para-BMeO**, and (c) **ortho-B**. DMSO/DCM = 95/5, v/v.

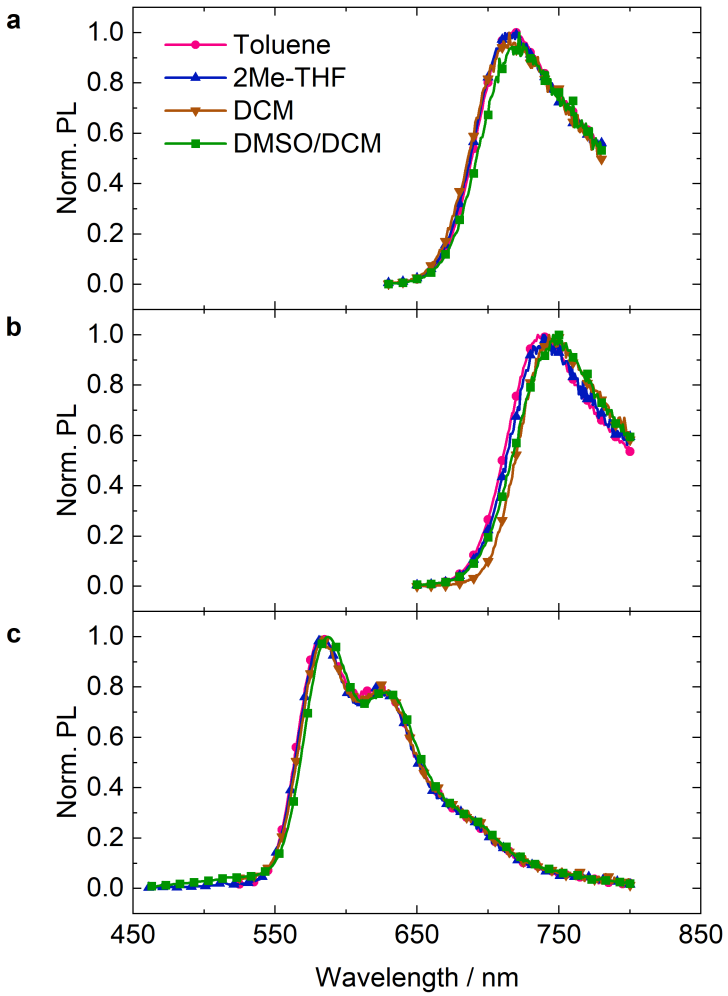

Figure S25. Photoluminescence spectra in various solvent (1.0×10^{-5} M for each) of (a) **para-B**, (b) **para-BMeO**, and (c) **ortho-B** excited at λ_{abs} in Table 1 for each condition.

Table S1. Optical properties of synthesized boron complexes

Compound	Condition	λ_{abs} / nm[a]	λ_{em} / nm[b]	Φ_{PL}[c]	τ / ns[d]	k_r / 10^7 s^{-1}[e]	k_{nr} / 10^9 s^{-1}[e]
para-B	Toluene	621	718	0.05	1.2	4	0.8
	2Me-THF	621	720	0.04	1.1	4	0.9
	DCM	613	715	0.04	1.2	3	0.8
	DMSO/DCM (99/1, v/v)	618	722	0.04	1.0	4	1
	Solid	n.d.	761[f]	0.03	n.d.[h]	n.d.	n.d.
para-BMeO	Toluene	641	739	0.04	0.8	5	1
	2Me-THF	639	743	0.03	0.7	4	1
	DCM	632	741	0.03	0.8	4	1
	DMSO/DCM (99/1, v/v)	640	750	0.03	0.6	5	2
	Solid	n.d.	788[g]	0.02	n.d.[h]	n.d.	n.d.
ortho-B	Toluene	515	584	0.02	0.5	4	2
	2Me-THF	516	584	0.02	0.5	4	2
	DCM	516	584	0.01	0.3	4	4
	DMSO/DCM (99/1, v/v)	519	587	0.03	0.7	5	2
	Solid	n.d.	615	0.06	n.d.[h]	n.d.	n.d.

[a]Absorption maximum in the longest wavelength region (concentration: 1.0×10^{-5} M). [b]Fluorescence maxima excited at λ_{abs} for each condition. [c]Absolute quantum yield determined with an integration sphere excited at λ_{abs}. [d]Averaged emission lifetime at λ_{em}. [e]$k_r = \Phi_{PL} / \tau$, $k_{nr} = (1 - \Phi_{PL}) / \tau$. [f]Fluorescence maxima excited at 618 nm. [g]Fluorescence maxima excited at 641 nm. [h]Not determined due to short lifetime. n.d.: Not determined.

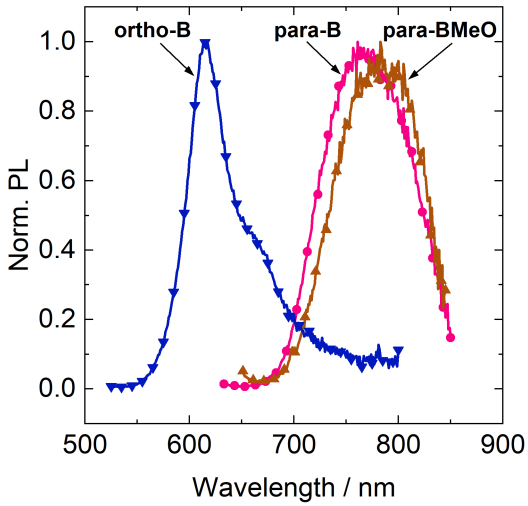

Figure S26. Photoluminescence spectra of solid states of **para-B**, **para-BMeO**, and **ortho-B** (excited at 618 nm for **para-B**, 641 nm for **para-BMeO**, and 476 nm for **ortho-B**).

Table S2. Optical properties of **para-B**, **para-BMeO**, and **ortho-B** at room temperature and 77 K[a]

Compound	Temp.	λ_{abs} / nm	λ_{PL} / nm	Φ_{PL}	τ / ns	k_r / 10^7 s^{-1}	k_{nr} / 10^9 s^{-1}
para-B	r.t.	621	720	0.04	1.1	4	0.9
	77 K	n.d.	693	0.11	2.3	5	0.4
para-BMeO	r.t.	693	743	0.03	0.7	4	1
	77 K	n.d.	715	0.07	1.6	4	0.6
ortho-B	r.t.	516	584	0.02	0.5	4	2
	77 K	n.d.	573	0.17	3.5	5	0.2

[a]Measured in 2-methyltetrahydrofurane 1.0×10^{-5} M solution.

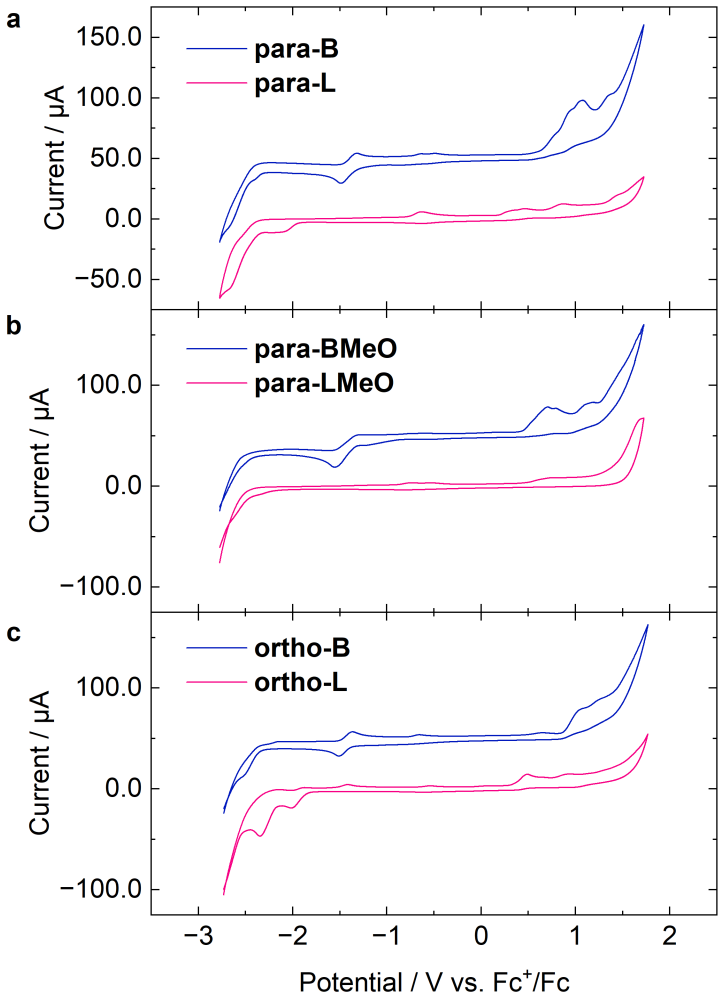

Figure S27. Voltammograms of (a) **para-L** and **para-B**, (b) **para-LMeO** and **para-BMeO**, and (c) **ortho-L** and **ortho-B** in CH_2Cl_2 (1.0×10^{-3} M) containing Bu_4NPF_6 (0.10 M) using a glassy carbon as a working electrode, a Pt wire as a counter electrode, an Ag/AgCl as a reference electrode, and Fc^+/Fc as an external standard at room temperature at a scan rate of 0.1 Vs^{-1}.

Table S3. Estimated frontier orbital energies of **para-L**, **para-B** and **para-BMeO** [a]

	HOMO / eV	LUMO / eV
para-L	–5.32	–3.15
para-B	–5.72	–3.81
para-BMeO	–5.55	–3.77

Energy levels of FMOs estimated from cyclic voltammetry measurements using the following empirical formula: E_{HOMO} / eV = –5.10 – $E_{ox,onset}$ / V; E_{LUMO} / eV = –5.10 – $E_{red,onset}$ / V, where $E_{ox,onset}$ and $E_{red,onset}$ were onset potentials for oxidation and reduction signals versus Fc/Fc^+, respectively.

4. DFT Calculations

The Gaussian 16 program package was used for computation. Optimization and time-dependent (TD)-DFT calculations were carried out at B3LYP/6-31+G(d,p) level of theory.

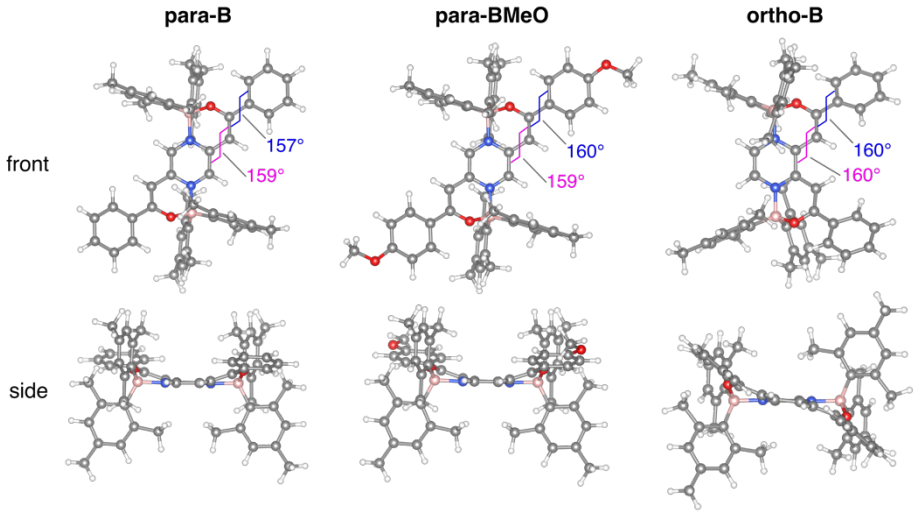

Figure S28. Optimized geometries of the boron complexes. Selected dihedral angles are shown in blue and magenta.

Table S4. Optimized geometry of **para-L** (enol-enol form) at the S_0 state

Center Number	Atomic Number	Coordinates (Angstroms)		
		x	y	z
1	6	-0.368022	-1.286498	-0.00024
2	6	-1.349626	-0.270575	-0.000251
3	7	-0.932762	1.028007	-0.000296
4	6	0.368051	1.286641	-0.000299
5	6	1.34965	0.270715	-0.000264
6	7	0.932791	-1.027867	-0.00025
7	6	2.760336	0.568226	-0.000232
8	6	-2.760309	-0.568105	-0.000204
9	6	3.751132	-0.37991	-0.000106
10	6	5.200742	-0.084323	0.000112
11	6	6.11947	-1.149981	-0.00176
12	6	7.493549	-0.906854	-0.001697
13	6	7.978697	0.402666	0.000293
14	6	7.074796	1.470678	0.002258
15	6	5.702666	1.23113	0.002192
16	8	3.46707	-1.696006	-0.000216
17	6	-3.751157	0.379983	-0.000128
18	6	-5.200746	0.084299	0.000101
19	6	-6.119547	1.149895	-0.001705
20	6	-7.49361	0.906673	-0.001624
21	6	-7.978667	-0.40288	0.000314
22	6	-7.074693	-1.470831	0.002209
23	6	-5.70258	-1.231189	0.002126
24	8	-3.467201	1.696102	-0.000296
25	1	-0.662021	-2.333642	-0.000208
26	1	0.66205	2.333785	-0.000314
27	1	3.033227	1.615156	-0.000426
28	1	-3.033166	-1.615044	-0.000337
29	1	5.744656	-2.166341	-0.003297
30	1	8.185401	-1.744171	-0.003204
31	1	9.04811	0.591959	0.000362
32	1	7.439839	2.493586	0.00392
33	1	5.026024	2.078647	0.003937
34	1	2.474128	-1.790806	-0.000372
35	1	-5.744801	2.16628	-0.003202
36	1	-8.185519	1.743943	-0.003076
37	1	-9.048067	-0.592246	0.000397
38	1	-7.439666	-2.493763	0.003825
39	1	-5.025878	-2.078658	0.003804
40	1	-2.474265	1.790998	-0.000451

Table S5. Result of TD-DFT calculation for **para-L** (enol-enol form) at the S_0 geometry

Excited State	Spin Multiplicity	Energy / eV	Wavelength / nm	*f*	Composition	Coefficient
1	Singlet-A	2.791	444.23	1.0028		
					HOMO -> LUMO	0.67998
					HOMO -> LUMO+1	-0.18981
2	Singlet-A	3.3048	375.16	0.6813		
					HOMO -> LUMO	0.19194
					HOMO -> LUMO+1	0.67666
3	Singlet-A	3.7046	334.68	0		
					HOMO-1 -> LUMO	-0.49469
					HOMO -> LUMO+2	0.49721

Table S6. Optimized geometry of **para-L** (keto-enol form) at the S_0 state

Center Number	Atomic Number	Coordinates (Angstroms)		
		x	y	z
1	6	0.187063	-0.782243	-1.376427
2	6	-0.810203	-0.732705	-0.368315
3	7	-0.473142	-1.107727	0.891208
4	6	0.783708	-1.501624	1.121196
5	6	1.750265	-1.544476	0.114545
6	7	1.428964	-1.177386	-1.143809
7	6	3.158721	-2.033513	0.366376
8	6	-2.157355	-0.300248	-0.648194
9	6	4.253507	-1.224451	-0.34353
10	6	4.448738	0.223673	-0.009138
11	8	4.97437	-1.780252	-1.158295
12	6	5.33496	0.972662	-0.802147
13	6	5.568547	2.317124	-0.523517
14	6	4.926024	2.931064	0.558
15	6	4.047649	2.194336	1.356445
16	6	3.807169	0.8486	1.072129
17	6	-3.150581	-0.227548	0.29488
18	6	-4.535169	0.213144	0.01739
19	8	-2.938532	-0.57887	1.574622
20	6	-5.546	-0.056523	0.957359
21	6	-6.863135	0.335414	0.716189
22	6	-7.19365	1.009893	-0.461676
23	6	-6.193592	1.294046	-1.397641
24	6	-4.877608	0.902099	-1.160716
25	1	-0.05481	-0.486592	-2.395484
26	1	1.021758	-1.794056	2.141822
27	1	3.356944	-2.052984	1.44511
28	1	3.267545	-3.057852	-0.004639
29	1	-2.384832	-0.040049	-1.67357
30	1	5.827904	0.477593	-1.632043
31	1	6.251019	2.888267	-1.146082
32	1	5.109536	3.979134	0.77676
33	1	3.549158	2.666022	2.198065
34	1	3.12017	0.292753	1.700812
35	1	-1.9861	-0.87205	1.652175
36	1	-5.288273	-0.5783	1.871501
37	1	-7.631815	0.113378	1.450714
38	1	-8.218544	1.317331	-0.647763
39	1	-6.437612	1.82982	-2.310301
40	1	-4.113844	1.154024	-1.888724

Table S7. Result of TD-DFT calculation for **para-L** (keto-enol form) at the S_0 geometry

Excited State	Spin Multiplicity	Energy / eV	Wavelength / nm	*f*	Composition	Coefficient
1	Singlet-A	3.3593	369.08	0.3071		
					HOMO -> LUMO	0.61745
					HOMO -> LUMO+1	-0.29338
					HOMO -> LUMO+2	0.15539
2	Singlet-A	3.4974	354.51	0.234		
					HOMO-1 -> LUMO+1	-0.25464
					HOMO -> LUMO	0.26822
					HOMO -> LUMO+1	0.57233
					HOMO -> LUMO+2	0.11938
3	Singlet-A	3.7686	328.99	0.0712		
					HOMO-6 -> LUMO+1	0.10566
					HOMO-5 -> LUMO+1	0.17324
					HOMO-1 -> LUMO	-0.10979
					HOMO-1 -> LUMO+1	0.56137
					HOMO-1 -> LUMO+2	0.10289
					HOMO -> LUMO+1	0.28464

Table S8. Optimized geometry of **para-L** (keto-keto form) at the S_0 state

Center Number	Atomic Number	Coordinates (Angstroms)		
		x	y	z
1	6	-0.100897	0.715739	-0.894281
2	6	-0.922769	0.782422	0.243493
3	7	-0.727889	-0.058888	1.268336
4	6	0.269395	-0.941495	1.153466
5	6	1.086598	-1.011342	0.017538
6	7	0.889846	-0.169535	-1.008936
7	6	2.182	-2.045861	-0.118873
8	6	3.463527	-1.537353	-0.793738
9	6	4.259757	-0.442352	-0.151243
10	6	5.321983	0.119231	-0.880159
11	6	6.105919	1.126701	-0.323241
12	6	5.845091	1.581711	0.974571
13	6	4.795271	1.026196	1.710223
14	6	4.00401	0.022002	1.148854
15	8	3.835723	-2.053582	-1.836194
16	6	-2.043148	1.796453	0.352006
17	6	-3.223842	1.468309	-0.577924
18	6	-4.276513	0.503389	-0.134249
19	8	-3.27728	2.00407	-1.677135
20	6	-5.390764	0.309145	-0.970753
21	6	-6.402009	-0.574388	-0.603943
22	6	-6.310587	-1.281695	0.601108
23	6	-5.204245	-1.101169	1.43478
24	6	-4.191233	-0.210252	1.073446
25	1	-0.253433	1.39702	-1.728015
26	1	0.42294	-1.615811	1.994028
27	1	2.42359	-2.462706	0.86649
28	1	1.828675	-2.871259	-0.745245
29	1	5.511738	-0.250406	-1.882232
30	1	6.920556	1.558326	-0.897312
31	1	6.457741	2.366026	1.409846
32	1	4.59154	1.374204	2.718546
33	1	3.191865	-0.3962	1.733769
34	1	-2.357444	1.853515	1.396071
35	1	-1.684866	2.78024	0.037158
36	1	-5.440794	0.863395	-1.902013
37	1	-7.260938	-0.71472	-1.253545
38	1	-7.099325	-1.971723	0.887248
39	1	-5.128168	-1.653283	2.366798
40	1	-3.330189	-0.093898	1.722762

Table S9. Result of TD-DFT calculation for **para-L** (keto-keto form) at the S_0 geometry

Excited State	Spin Multiplicity	Energy / eV	Wavelength / nm	*f*	Composition	Coefficient
1	Singlet-A	3.6167	342.81	0.0132		
					HOMO-7 -> LUMO	-0.15133
					HOMO-4 -> LUMO	0.19101
					HOMO-2 -> LUMO	-0.11292
					HOMO-1 -> LUMO	0.45992
					HOMO-1 -> LUMO+2	0.14333
					HOMO -> LUMO	-0.39006
2	Singlet-A	3.6882	336.16	0.0007		
					HOMO-6 -> LUMO+1	-0.19036
					HOMO-6 -> LUMO+2	-0.10087
					HOMO-4 -> LUMO+1	0.13857
					HOMO-1 -> LUMO+1	0.22517
					HOMO -> LUMO+1	0.54871
					HOMO -> LUMO+2	0.18142
3	Singlet-A	3.9069	317.35	0.016		
					HOMO-6 -> LUMO	0.18161
					HOMO-6 -> LUMO+1	0.11213
					HOMO-6 -> LUMO+2	-0.1438
					HOMO-2 -> LUMO	0.15415
					HOMO-2 -> LUMO+1	0.10216
					HOMO-2 -> LUMO+2	-0.13251
					HOMO-1 -> LUMO	0.32332
					HOMO-1 -> LUMO+2	-0.19582
					HOMO -> LUMO	0.32112
					HOMO -> LUMO+2	-0.31301

Table S10. Optimized geometry of **para-LMeO** (enol-enol form) at the S_0 state

Center Number	Atomic Number	Coordinates (Angstroms)		
		x	y	z
1	6	-0.442167	-1.262651	-0.000236
2	6	-1.364387	-0.192079	-0.000208
3	7	-0.871476	1.080385	-0.000293
4	6	0.442173	1.262693	-0.000282
5	6	1.364392	0.19212	-0.00021
6	7	0.871482	-1.080344	-0.00025
7	6	2.789179	0.407198	-0.000207
8	6	-2.789174	-0.407161	-0.000199
9	6	3.72487	-0.597084	-0.000138
10	6	5.185607	-0.391285	-0.00009
11	6	6.046493	-1.508982	-0.003913
12	6	7.425779	-1.356533	-0.004185
13	6	7.99555	-0.074529	-0.000542
14	6	7.158746	1.051153	0.003467
15	6	5.774291	0.883297	0.003689
16	8	3.361805	-1.894821	-0.000346
17	6	-3.724877	0.597112	-0.00018
18	6	-5.185611	0.391292	-0.000114
19	6	-6.046513	1.508976	-0.003859
20	6	-7.425797	1.356507	-0.004106
21	6	-7.995549	0.074494	-0.000517
22	6	-7.158728	-1.051176	0.003407
23	6	-5.774276	-0.8833	0.003604
24	8	-3.361835	1.894855	-0.000455
25	8	9.358519	-0.025349	-0.001169
26	6	9.997591	1.246296	0.003024
27	8	-9.358517	0.025294	-0.001114
28	6	-9.997571	-1.24636	0.003022
29	1	-0.796357	-2.291129	-0.000253
30	1	0.796362	2.291171	-0.000336
31	1	3.122256	1.436831	-0.000508
32	1	-3.122244	-1.436795	-0.000439
33	1	5.615705	-2.502982	-0.006741
34	1	8.084196	-2.219103	-0.007204
35	1	7.568349	2.054071	0.006536
36	1	5.15615	1.774599	0.007179
37	1	2.364584	-1.929087	-0.000506
38	1	-5.61574	2.502982	-0.006643
39	1	-8.084226	2.219067	-0.007061
40	1	-7.568316	-2.0541	0.006424
41	1	-5.156121	-1.774593	0.007016
42	1	-2.364614	1.929143	-0.000641
43	1	11.068372	1.039806	0.002068
44	1	9.737851	1.826539	-0.891079
45	1	9.738257	1.820421	0.901181
46	1	-11.068355	-1.039886	0.002102
47	1	-9.737843	-1.826549	-0.89112
48	1	-9.738207	-1.820532	0.901141

Table S11. Result of TD-DFT calculation for **para-LMeO** (enol-enol form) at the S_0 geometry

Excited State	Spin Multiplicity	Energy / eV	Wavelength / nm	*f*	Composition	Coefficient
1	Singlet-A	2.7003	459.14	1.0608		
					HOMO -> LUMO	0.68204
					HOMO -> LUMO+1	-0.18102
2	Singlet-A	3.2217	384.84	0.8619		
					HOMO -> LUMO	0.18203
					HOMO -> LUMO+1	0.67882
3	Singlet-A	3.5637	347.91	0		
					HOMO-1 -> LUMO	0.61823
					HOMO-1 -> LUMO+1	-0.1032
					HOMO -> LUMO+2	-0.31496

Table S12. Optimized geometry of **para-LMeO** (keto-enol form) at the S_0 state

Center Number	Atomic Number	Coordinates (Angstroms)		
		x	y	z
1	6	0.363292	-1.505617	-1.113149
2	6	-0.526422	-1.166422	-0.061551
3	7	-0.098261	-1.311132	1.217342
4	6	1.143458	-1.762389	1.422807
5	6	2.004825	-2.0908	0.373571
6	7	1.590668	-1.955734	-0.903737
7	6	3.393135	-2.640502	0.610834
8	6	-1.859848	-0.678068	-0.318481
9	6	4.479138	-2.07333	-0.317787
10	6	4.816515	-0.622511	-0.268019
11	8	5.072935	-2.833549	-1.070622
12	6	5.723464	-0.110563	-1.219193
13	6	6.088908	1.224386	-1.212037
14	6	5.559225	2.094375	-0.240733
15	6	4.660536	1.605061	0.717469
16	6	4.297392	0.256544	0.691604
17	6	-2.756842	-0.336047	0.663019
18	6	-4.121284	0.147607	0.393862
19	8	-2.449599	-0.437987	1.968413
20	6	-5.006238	0.313209	1.406302
21	6	-6.397937	0.829034	1.155682
22	6	-6.916233	0.455732	-0.233912
23	6	-5.840863	0.683109	-1.275343
24	6	-4.544609	0.502617	-0.975741
25	8	5.978263	3.386227	-0.314546
26	6	5.482126	4.327008	0.633719
27	8	-8.091382	1.229602	-0.472864
28	6	-8.944751	0.707484	-1.477769
29	1	0.045931	-1.400009	-2.148844
30	1	1.456702	-1.866389	2.459655
31	1	3.680531	-2.478381	1.656942
32	1	3.396919	-3.720925	0.433818
33	1	-2.160194	-0.602308	-1.354834
34	1	6.129076	-0.790466	-1.9608
35	1	6.78224	1.624964	-1.944355
36	1	4.241303	2.254185	1.476507
37	1	3.59823	-0.097917	1.441147
38	1	-1.518382	-0.791574	2.031099
39	1	-4.695483	0.121146	2.427528
40	1	-6.394044	1.92966	1.233746
41	1	-7.094651	0.469365	1.918772
42	1	-7.193417	-0.61598	-0.239913
43	1	-6.144428	0.968578	-2.278615
44	1	-3.788241	0.658479	-1.738188
45	1	5.948844	5.278397	0.377387
46	1	4.39207	4.424412	0.563998
47	1	5.76275	4.046546	1.656103
48	1	-9.811584	1.369803	-1.529941
49	1	-8.462135	0.681703	-2.465321
50	1	-9.282546	-0.309073	-1.225101

Table S13. Result of TD-DFT calculation for **para-LMeO** (keto-enol form) at the S_0 geometry

Excited State	Spin Multiplicity	Energy / eV	Wavelength / nm	*f*	Composition	Coefficient
1	Singlet-A	3.3162	373.88	0.357		
					HOMO -> LUMO	0.64436
					HOMO -> LUMO+1	0.23912
					HOMO -> LUMO+2	0.14668
2	Singlet-A	3.6079	343.65	0.1653		
					HOMO-3 -> LUMO+1	0.22927
					HOMO-3 -> LUMO+2	-0.14677
					HOMO-1 -> LUMO+1	-0.1043
					HOMO -> LUMO	-0.18601
					HOMO -> LUMO+1	0.57425
					HOMO -> LUMO+2	-0.1507
3	Singlet-A	3.8122	325.23	0.1217		
					HOMO-4 -> LUMO	-0.11766
					HOMO-3 -> LUMO	-0.23705
					HOMO-3 -> LUMO+1	-0.40684
					HOMO-3 -> LUMO+2	0.16842
					HOMO -> LUMO	-0.15183
					HOMO -> LUMO+1	0.27561
					HOMO -> LUMO+2	0.2876

Table S14. Optimized geometry of **para-LMeO** (keto-keto form) at the S_0 state

Center Number	Atomic Number	Coordinates (Angstroms)		
		x	y	z
1	6	0.151597	-0.520425	-1.119963
2	6	0.791104	-1.065707	0.006534
3	7	0.614317	-0.516127	1.216016
4	6	-0.188287	0.550529	1.290216
5	6	-0.825525	1.095628	0.167732
6	7	-0.64536	0.545838	-1.043491
7	6	-1.696473	2.32877	0.262186
8	6	1.682685	-2.286458	-0.103269
9	6	-2.973694	2.286679	-0.59201
10	6	-4.021096	1.265191	-0.309498
11	8	-3.123738	3.117461	-1.477422
12	6	-5.118739	1.1668	-1.189716
13	6	-6.131458	0.249596	-0.969064
14	6	-6.080605	-0.599692	0.152089
15	6	-5.001264	-0.514637	1.042631
16	6	-3.984242	0.411854	0.801095
17	6	2.942204	-2.025775	-0.944862
18	6	4.116939	-1.344211	-0.316856
19	6	5.273918	-1.282078	-1.017353
20	6	6.51648	-0.688927	-0.430407
21	6	6.266067	0.34864	0.668831
22	6	5.073257	-0.02291	1.524009
23	6	4.071764	-0.781278	1.04129
24	8	-7.121368	-1.465235	0.284163
25	6	-7.137546	-2.35994	1.392906
26	8	6.072458	1.609827	0.00485
27	6	6.04665	2.737138	0.865293
28	8	2.956229	-2.383346	-2.115917
29	1	0.291818	-0.962376	-2.10375
30	1	-0.328719	0.986596	2.277706
31	1	-1.958424	2.516684	1.310565
32	1	-1.135355	3.197693	-0.096148
33	1	1.937026	-2.615098	0.907354
34	1	1.147378	-3.09357	-0.611351
35	1	-5.150187	1.828597	-2.048665
36	1	-6.975514	0.16534	-1.645747
37	1	-4.941032	-1.155322	1.913931
38	1	-3.158458	0.45711	1.503009
39	1	5.313086	-1.722142	-2.009921
40	1	7.136007	-0.230055	-1.208821
41	1	7.112732	-1.516395	-0.010988
42	1	7.167225	0.432714	1.296865
43	1	5.003698	0.390693	2.52638
44	1	3.198447	-0.965251	1.658937
45	1	-8.050595	-2.946065	1.285786
46	1	-6.269453	-3.029844	1.375739
47	1	-7.163594	-1.814233	2.343834
48	1	6.022096	3.620396	0.223427
49	1	5.159081	2.746187	1.512018
50	1	6.948976	2.777983	1.495903

Table S15. Result of TD-DFT calculation for **para-LMeO** (keto-keto form) at the S_0 geometry

Excited State	Spin Multiplicity	Energy / eV	Wavelength / nm	*f*	Composition	Coefficient
1	Singlet-A	3.5401	350.23	0.0085		
					HOMO-7 -> LUMO	0.14631
					HOMO-4 -> LUMO	-0.13988
					HOMO-3 -> LUMO	0.5256
					HOMO-3 -> LUMO+5	0.11325
					HOMO-2 -> LUMO	-0.31682
					HOMO-1 -> LUMO	0.113
					HOMO -> LUMO	0.14797
2	Singlet-A	3.7729	328.62	0.0003		
					HOMO-5 -> LUMO+2	-0.13101
					HOMO-4 -> LUMO+2	0.18273
					HOMO-3 -> LUMO+1	0.12674
					HOMO-3 -> LUMO+2	-0.13046
					HOMO-2 -> LUMO+1	0.39536
					HOMO-2 -> LUMO+2	-0.45845
3	Singlet-A	3.8716	320.24	0.0602		
					HOMO-5 -> LUMO	-0.13575
					HOMO-5 -> LUMO+1	-0.1744
					HOMO-4 -> LUMO	0.15278
					HOMO-4 -> LUMO+1	0.19397
					HOMO-3 -> LUMO	0.14834
					HOMO-3 -> LUMO+1	0.10849
					HOMO-2 -> LUMO	0.31484
					HOMO-2 -> LUMO+1	0.2155
					HOMO-2 -> LUMO+2	0.23749
					HOMO -> LUMO	0.35027

Table S16. Optimized geometry of **para-B** at the S_0 state

Center Number	Atomic Number	Coordinates (Angstroms)		
		x	y	z
1	6	0.4467	-1.260237	0.046502
2	6	-0.938102	-1.017406	0.027544
3	7	-1.360921	0.289473	0.064794
4	6	-0.446698	1.260232	0.046335
5	6	0.938101	1.017397	0.027381
6	7	1.360916	-0.289478	0.064808
7	6	1.88603	2.071943	-0.111599
8	6	3.158563	1.799331	-0.559845
9	6	4.124752	2.853453	-0.94036
10	6	3.701631	4.142285	-1.314745
11	6	4.631549	5.122532	-1.656266
12	6	5.999782	4.832803	-1.632185
13	6	6.4299	3.553675	-1.269392
14	6	5.501518	2.569617	-0.930129
15	6	-1.886039	-2.071972	-0.111262
16	6	-3.158529	-1.799394	-0.559657
17	6	-4.124701	-2.853545	-0.940131
18	6	-5.50147	-2.569719	-0.929963
19	6	-6.42983	-3.553807	-1.269194
20	6	-5.999686	-4.832954	-1.631896
21	6	-4.631451	-5.12267	-1.65592
22	6	-3.701553	-4.142391	-1.314428
23	5	2.999643	-0.634374	0.014669
24	5	-2.999597	0.634331	0.014647
25	8	3.56909	0.557577	-0.733415
26	8	-3.56902	-0.557649	-0.733379
27	6	3.113857	-1.995894	-0.893076
28	6	3.213079	-3.290386	-0.306706
29	6	3.326146	-4.436325	-1.110937
30	6	3.340886	-4.372708	-2.503531
31	6	3.187581	-3.111827	-3.082163
32	6	3.062528	-1.942777	-2.318014
33	6	2.853083	-0.662706	-3.11147
34	6	3.190067	-3.547745	1.19218
35	6	3.5151	-5.611615	-3.350517
36	6	3.785107	-0.610716	1.461951
37	6	5.202573	-0.782075	1.393045
38	6	5.997026	-0.674472	2.542405
39	6	5.458449	-0.413336	3.803128
40	6	4.073996	-0.278963	3.880044
41	6	3.242413	-0.370491	2.751397
42	6	1.75833	-0.226775	3.030795
43	6	5.945985	-1.161962	0.121044
44	6	6.338845	-0.265144	5.022032
45	6	-3.113899	1.995818	-0.893158
46	6	-3.213106	3.290318	-0.306846
47	6	-3.326239	4.43623	-1.111135
48	6	-3.34104	4.372557	-2.503711
49	6	-3.187776	3.111637	-3.082302
50	6	-3.062675	1.942635	-2.318114
51	6	-2.853297	0.662518	-3.111519
52	6	-3.190014	3.547759	1.192024
53	6	-3.515158	5.611396	-3.350821
54	6	-3.785052	0.610766	1.461933
55	6	-5.202548	0.782111	1.393005
56	6	-5.996984	0.674663	2.542358
57	6	-5.458384	0.41371	3.803141
58	6	-4.073963	0.279294	3.880056
59	6	-3.242365	0.370673	2.75137
60	6	-1.75829	0.226875	3.030783
61	6	-5.945938	1.161803	0.12093
62	6	-6.338851	0.265969	5.02205
63	1	0.818208	-2.275812	0.009631
64	1	-0.818211	2.2758	0.009337
65	1	1.544148	3.089969	0.012313
66	1	2.642854	4.373703	-1.367697
67	1	4.28827	6.10969	-1.951421
68	1	6.723441	5.597297	-1.899608
69	1	7.490619	3.321554	-1.247298
70	1	5.832965	1.580476	-0.639927
71	1	-1.544175	-3.089985	0.012807
72	1	-5.832934	-1.580561	-0.639838
73	1	-7.490553	-3.321698	-1.247149
74	1	-6.723331	-5.597469	-1.899297
75	1	-4.288152	-6.109842	-1.951006
76	1	-2.642771	-4.373796	-1.367337
77	1	3.401154	-5.408131	-0.626343
78	1	3.150605	-3.031477	-4.167125
79	1	2.624402	-0.905312	-4.153563
80	1	2.025857	-0.059631	-2.726084
81	1	3.739096	-0.022097	-3.100625
82	1	2.421313	-2.973665	1.716333
83	1	2.997497	-4.607938	1.383809
84	1	4.139732	-3.29048	1.670699
85	1	3.190293	-6.510494	-2.816877
86	1	2.944227	-5.543673	-4.282534
87	1	4.567992	-5.756665	-3.624535
88	1	7.073156	-0.809614	2.445923
89	1	3.616181	-0.095005	4.850224
90	1	1.581739	-0.163354	4.107826
91	1	1.336377	0.678401	2.586327
92	1	1.177604	-1.078891	2.664265
93	1	5.570807	-0.658457	-0.769061
94	1	7.011037	-0.930031	0.224357
95	1	5.866176	-2.23837	-0.071591
96	1	7.184034	-0.961125	4.992924
97	1	6.755161	0.748336	5.088976
98	1	5.778932	-0.450283	5.944169
99	1	-3.40127	5.408055	-0.626588
100	1	-3.150881	3.031226	-4.167266
101	1	-2.624746	0.905064	-4.153654
102	1	-2.02601	0.059487	-2.726192
103	1	-3.739291	0.021887	-3.100524
104	1	-2.421209	2.973728	1.716158
105	1	-2.997458	4.607967	1.383584
106	1	-4.139642	3.290495	1.670617
107	1	-3.194346	6.510791	-2.815657
108	1	-2.9408	5.545191	-4.280837
109	1	-4.567388	5.754062	-3.628593
110	1	-7.073121	0.809767	2.445857
111	1	-3.616151	0.095396	4.850244
112	1	-1.581709	0.163475	4.107816
113	1	-1.336387	-0.678338	2.586342
114	1	-1.177512	1.078948	2.664235
115	1	-5.570587	0.658361	-0.769135
116	1	-7.010952	0.929662	0.224165
117	1	-5.86633	2.238228	-0.071711
118	1	-7.180084	0.966885	4.99612
119	1	-6.760974	-0.745326	5.085436
120	1	-5.777302	0.444492	5.944482

Table S18. Result of TD-DFT calculation for **para-B** at the S_0 geometry

Excited State	Spin Multiplicity	Energy / eV	Wavelength / nm	*f*	Composition	Coefficient
1	Singlet-A	1.9559	633.9	0.1796		
					HOMO -> LUMO	0.6995
2	Singlet-A	2.2322	555.45	0.0024		
					HOMO-1 -> LUMO	0.70006
3	Singlet-A	2.2444	552.42	0.006		
					HOMO-2 -> LUMO	0.69953
4	Singlet-A	2.4022	516.13	0.0004		
					HOMO-3 -> LUMO	0.69583
5	Singlet-A	2.4032	515.92	0.0135		
					HOMO-5 -> LUMO	0.5181
					HOMO-4 -> LUMO	0.47266
6	Singlet-A	2.4559	504.84	0.0018		
					HOMO-5 -> LUMO	-0.4759
					HOMO-4 -> LUMO	0.51364
7	Singlet-A	2.4562	504.77	0		
					HOMO-6 -> LUMO	0.69982
8	Singlet-A	2.5694	482.55	0.0002		
					HOMO-7 -> LUMO	0.70394
9	Singlet-A	2.5766	481.2	0.0011		
					HOMO-8 -> LUMO	0.70444
10	Singlet-A	2.9182	424.86	0.0038		
					HOMO-9 -> LUMO	0.69458
11	Singlet-A	2.9764	416.56	0.6973		
					HOMO -> LUMO+1	0.69154
12	Singlet-A	3.2511	381.36	0.0057		
					HOMO-1 -> LUMO+1	0.69976
13	Singlet-A	3.2685	379.34	0.0162		
					HOMO-2 -> LUMO+1	0.69812
14	Singlet-A	3.4187	362.66	0.0013		
					HOMO-3 -> LUMO+1	0.69968
15	Singlet-A	3.4246	362.04	0.0209		
					HOMO-5 -> LUMO+1	0.42727
					HOMO-4 -> LUMO+1	0.5579
16	Singlet-A	3.4696	357.34	0.0255		
					HOMO-10 -> LUMO	-0.26806
					HOMO-5 -> LUMO+1	0.51292
					HOMO-4 -> LUMO+1	-0.38956
17	Singlet-A	3.4749	356.8	0.2329		
					HOMO-12 -> LUMO	0.17257
					HOMO-10 -> LUMO	0.61402
					HOMO-5 -> LUMO+1	0.22328
					HOMO-4 -> LUMO+1	-0.16732
18	Singlet-A	3.486	355.67	0.0003		
					HOMO-6 -> LUMO+1	0.70362
19	Singlet-A	3.5708	347.21	0.0002		
					HOMO-13 -> LUMO	0.27237
					HOMO-11 -> LUMO	0.59732
					HOMO -> LUMO+2	-0.20958
20	Singlet-A	3.5855	345.79	0.0005		
					HOMO-7 -> LUMO+1	0.69799

Table S20. Optimized geometry of **para-BMeO** at the S_0 state

Center Number	Atomic Number	Coordinates (Angstroms)		
		x	y	z
1	6	0.052456	-1.335905	0.196955
2	6	-1.198507	-0.694165	0.176513
3	7	-1.213742	0.68039	0.215629
4	6	-0.052409	1.335925	0.196995
5	6	1.198554	0.694185	0.176539

6	7	1.21379	-0.680372	0.215615
7	6	2.415993	1.419301	0.03883
8	6	3.551781	0.782763	-0.41266
9	6	4.783046	1.495942	-0.798234
10	6	6.01246	0.806792	-0.840469
11	6	7.187096	1.457445	-1.186133
12	6	7.168992	2.823817	-1.509927
13	6	5.954599	3.525881	-1.484698
14	6	4.781122	2.859346	-1.133176
15	6	-2.415948	-1.419273	0.038748
16	6	-3.551728	-0.782712	-0.412721
17	6	-4.78299	-1.495871	-0.798323
18	6	-6.01243	-0.806752	-0.840382
19	6	-7.187067	-1.457403	-1.186038
20	6	-7.16894	-2.823736	-1.510002
21	6	-5.95452	-3.525759	-1.484966
22	6	-4.781039	-2.859227	-1.133444
23	5	2.675331	-1.491986	0.166498
24	5	-2.675251	1.491996	0.166534
25	8	3.570693	-0.526701	-0.586734
26	8	-3.570635	0.526762	-0.586752
27	6	2.383168	-2.831965	-0.735622
28	6	2.095071	-4.095245	-0.14393
29	6	1.867246	-5.227795	-0.942969
30	6	1.903156	-5.178234	-2.335666
31	6	2.128751	-3.930885	-2.919939
32	6	2.351898	-2.773086	-2.160917
33	6	2.529058	-1.491735	-2.960141
34	6	1.993128	-4.326727	1.355923
35	6	1.707384	-6.417767	-3.177169
36	6	3.435069	-1.699195	1.614146
37	6	4.737693	-2.283516	1.546019
38	6	5.529262	-2.413997	2.695089
39	6	5.093255	-2.002239	3.955194
40	6	3.81109	-1.462874	4.031729
41	6	2.989241	-1.305862	2.903131
42	6	1.615393	-0.726224	3.181389
43	6	5.334507	-2.869959	0.275271
44	6	5.979001	-2.118747	5.173742
45	6	-2.38313	2.832052	-0.735481
46	6	-2.09512	4.095335	-0.143685
47	6	-1.867415	5.227944	-0.942626
48	6	-1.903365	5.178483	-2.335353
49	6	-2.128833	3.931177	-2.919704
50	6	-2.351865	2.773279	-2.160748
51	6	-2.528901	1.491982	-2.960086
52	6	-1.993129	4.32666	1.356187
53	6	-1.707843	6.418176	-3.176678
54	6	-3.435003	1.699075	1.614195
55	6	-2.989208	1.305615	2.903138
56	6	-3.811135	1.462425	4.031721
57	6	-5.093309	2.001751	3.9552
58	6	-5.529281	2.413651	2.695118
59	6	-4.737656	2.283343	1.546078
60	6	-5.334418	2.869883	0.275346
61	6	-1.615337	0.726025	3.181395
62	6	-5.979088	2.118264	5.173726
63	8	8.371089	3.373087	-1.83842
64	6	8.426258	4.756661	-2.171611
65	8	-8.371047	-3.373003	-1.838469
66	6	-8.426222	-4.756557	-2.171739
67	1	0.105742	-2.415971	0.16063
68	1	-0.105694	2.415993	0.160709
69	1	2.390034	2.492698	0.164805
70	1	6.035213	-0.244483	-0.582418
71	1	8.134981	0.929882	-1.208313
72	1	5.908553	4.576008	-1.7465
73	1	3.849225	3.414911	-1.149584
74	1	-2.390002	-2.492674	0.164699
75	1	-6.035192	0.244492	-0.5822
76	1	-8.134973	-0.929874	-1.208083
77	1	-5.908454	-4.575847	-1.746921
78	1	-3.849117	-3.414749	-1.149999
79	1	1.651698	-6.176198	-0.454025
80	1	2.118958	-3.848421	-4.00538
81	1	3.564437	-1.140481	-2.950362
82	1	1.916587	-0.67003	-2.578059
83	1	2.239151	-1.661064	-4.001584
84	1	2.975356	-4.363699	1.83655
85	1	1.491239	-5.279618	1.551164
86	1	1.430824	-3.545936	1.874838
87	1	2.671728	-6.865211	-3.450317
88	1	1.180311	-6.190229	-4.109774
89	1	1.134815	-7.180414	-2.639644
90	1	6.516998	-2.862104	2.598735
91	1	3.429046	-1.148944	5.001416
92	1	0.80737	-1.367274	2.815734
93	1	1.482672	0.2623	2.734087
94	1	1.465621	-0.61066	4.258209
95	1	4.94561	-3.878323	0.090227
96	1	6.421538	-2.95564	0.37483
97	1	5.117198	-2.284941	-0.617395
98	1	5.389882	-2.130428	6.096256
99	1	6.675087	-1.272509	5.239873
100	1	6.58215	-3.03254	5.144942
101	1	-1.651911	6.176328	-0.453619
102	1	-2.119037	3.848787	-4.005148
103	1	-3.564291	1.140744	-2.950502
104	1	-1.916507	0.670241	-2.577969
105	1	-2.23883	1.661383	-4.001472
106	1	-1.491324	5.279577	1.551512
107	1	-1.43072	3.545861	1.874979
108	1	-2.975333	4.363474	1.836873
109	1	-2.672166	6.867988	-3.445994
110	1	-1.184639	6.190116	-4.111316
111	1	-1.131662	7.179191	-2.640681
112	1	-3.429145	1.14835	5.00138
113	1	-6.517043	2.861706	2.598764
114	1	-4.945619	3.878321	0.090486
115	1	-5.116953	2.285015	-0.617381
116	1	-6.421469	2.955428	0.374807
117	1	-1.465547	0.610507	4.258218
118	1	-1.48259	-0.262516	2.734128
119	1	-0.807338	1.367081	2.815709
120	1	-5.390185	2.126522	6.096408
121	1	-6.579716	3.033781	5.14659
122	1	-6.677543	1.273843	5.237972
123	1	9.474279	4.967325	-2.386456
124	1	7.82091	4.977145	-3.059304
125	1	8.092746	5.381489	-1.33414
126	1	-9.474266	-4.96724	-2.386453
127	1	-7.820991	-4.976969	-3.059529
128	1	-8.092577	-5.381429	-1.334354

Table S22. Result of TD-DFT calculation for **para-BMeO** at the S_0 geometry

Excited State	Spin Multiplicity	Energy / eV	Wavelength / nm	*f*	Composition	Coefficient
1	Singlet-A	1.8082	685.69	0.2244		
					HOMO-10 -> LUMO	0.10883
					HOMO -> LUMO	0.69445
2	Singlet-A	2.9476	420.63	0.0000		
					HOMO-11 -> LUMO	-0.28034
					HOMO-9 -> LUMO	-0.27886
					HOMO-7 -> LUMO	0.15733
					HOMO-6 -> LUMO	-0.19866
					HOMO-1 -> LUMO	0.50519
3	Singlet-A	3.0351	408.50	0.0108		
					HOMO-4 -> LUMO	-0.19196
					HOMO-2 -> LUMO	0.66760

Table S23. Optimized geometry of **ortho-L** (enol-enol form) at the S_0 state

Center Number	Atomic Number	Atomic Type	Coordinates (Angstroms)		
			x	y	z
1	6	0	0.724731	1.71168	-0.035386
2	6	0	-0.724695	1.711661	-0.035387
3	7	0	-1.380533	2.89175	-0.051106
4	6	0	-0.692294	4.044387	-0.069734
5	6	0	0.692286	4.044395	-0.069764
6	7	0	1.380549	2.89177	-0.051142
7	6	0	1.512666	0.503481	-0.016329
8	6	0	-1.512619	0.503467	-0.016365
9	6	0	-2.887766	0.486553	-0.025536
10	6	0	-3.69967	-0.750564	-0.001168
11	6	0	2.887806	0.48655	-0.025548
12	6	0	3.699675	-0.750574	-0.001142
13	6	0	5.055726	-0.675891	0.364565
14	6	0	5.843096	-1.826547	0.41212
15	6	0	5.295148	-3.069858	0.086667
16	6	0	3.951262	-3.15347	-0.292285
17	6	0	3.161569	-2.006133	-0.337891
18	6	0	-5.055679	-0.675864	0.364696
19	6	0	-5.843087	-1.826495	0.412235
20	6	0	-5.295224	-3.069796	0.086606
21	6	0	-3.951384	-3.153423	-0.292506
22	6	0	-3.161651	-2.006113	-0.338093
23	8	0	-3.612109	1.613035	-0.035098
24	8	0	3.612185	1.613018	-0.035205
25	1	0	-1.266604	4.965718	-0.083012
26	1	0	1.26658	4.965736	-0.083076
27	1	0	0.999803	-0.443892	0.033065
28	1	0	-0.99975	-0.443907	0.032915
29	1	0	5.4798	0.28965	0.614467
30	1	0	6.886696	-1.750792	0.70347
31	1	0	5.909351	-3.964945	0.120578
32	1	0	3.519979	-4.112981	-0.562394
33	1	0	2.129314	-2.088675	-0.661334
34	1	0	-5.479686	0.28967	0.614734
35	1	0	-6.886651	-1.750726	0.703711
36	1	0	-5.909457	-3.964863	0.120503
37	1	0	-3.520169	-4.112924	-0.562758
38	1	0	-2.12944	-2.088671	-0.661672
39	1	0	-2.955132	2.376945	-0.034746
40	1	0	2.955281	2.376912	-0.034829

Table S24. Result of TD-DFT calculation for **ortho-L** (enol-enol form) at the S_0 geometry

Excited State	Spin Multiplicity	Energy / eV	Wavelength / nm	*f*	Composition	Coefficient
1	Singlet-A	3.022	410.27	0.1815		
					HOMO-1 -> LUMO+1	0.14405
					HOMO -> LUMO	0.68931
2	Singlet-A	3.1876	388.96	0.6029		
					HOMO -> LUMO+1	0.70152
3	Singlet-A	3.7182	333.45	0.2966		
					HOMO-1 -> LUMO	0.69937

Table S25. Optimized geometry of **ortho-L** (keto-enol form) at the S_0 state

Center Number	Atomic Number	Atomic Type	Coordinates (Angstroms)		
			x	y	z
1	6	0	0.303983	3.405357	0.375895
2	6	0	1.580581	3.078277	-0.059882
3	7	0	1.859617	1.851369	-0.534051
4	6	0	0.884025	0.951903	-0.583106
5	6	0	-0.444374	1.271221	-0.151508
6	7	0	-0.693253	2.514566	0.329857
7	6	0	-1.536866	0.329236	-0.211943
8	6	0	1.218933	-0.417707	-1.139964
9	6	0	-2.814207	0.61079	0.212316
10	6	0	-3.940939	-0.346417	0.144961
11	8	0	-3.147104	1.808056	0.712326
12	6	0	-5.257199	0.130927	0.277997
13	6	0	-6.340959	-0.744442	0.204519
14	6	0	-6.13092	-2.111227	0.005856
15	6	0	-4.825296	-2.598402	-0.115251
16	6	0	-3.740951	-1.726117	-0.04486
17	6	0	2.710209	-0.630728	-1.416292
18	6	0	3.647015	-0.889735	-0.276768
19	8	0	3.107895	-0.634391	-2.572163
20	6	0	5.008858	-1.076929	-0.567582
21	6	0	5.921029	-1.333513	0.453256
22	6	0	5.484339	-1.408811	1.78092
23	6	0	4.132249	-1.224213	2.081241
24	6	0	3.21849	-0.965306	1.058089
25	1	0	0.067851	4.391591	0.76655
26	1	0	2.394394	3.796832	-0.032082
27	1	0	-1.346557	-0.640331	-0.646961
28	1	0	0.849743	-1.19787	-0.462646
29	1	0	0.707641	-0.558025	-2.099159
30	1	0	-2.318618	2.377352	0.686968
31	1	0	-5.41854	1.191197	0.433503
32	1	0	-7.350917	-0.357232	0.302889
33	1	0	-6.97477	-2.792763	-0.048452
34	1	0	-4.650897	-3.660985	-0.25655
35	1	0	-2.736148	-2.128611	-0.117029
36	1	0	5.32767	-1.014933	-1.60265
37	1	0	6.971752	-1.475107	0.2175
38	1	0	6.195127	-1.609966	2.577406
39	1	0	3.789417	-1.280123	3.110197
40	1	0	2.173973	-0.816863	1.311209

Table S26. Result of TD-DFT calculation for **ortho-L** (keto-enol form) at the S_0 geometry

Excited State	Spin Multiplicity	Energy / eV	Wavelength / nm	*f*	Composition	Coefficient
1	Singlet-A	3.5123	353	0.5287		
					HOMO -> LUMO	0.67701
					HOMO -> LUMO+2	0.18935
2	Singlet-A	3.6464	340.02	0.0049		
					HOMO -> LUMO+1	0.70485
3	Singlet-A	3.7134	333.88	0.0001		
					HOMO-5 -> LUMO+1	-0.20615
					HOMO-4 -> LUMO+1	0.12448
					HOMO-2 -> LUMO+1	0.13491
					HOMO-1 -> LUMO+1	0.63497

Table S27. Optimized geometry of **ortho-L** (keto-keto form) at the S_0 state

Center Number	Atomic Number	Atomic Type	Coordinates (Angstroms)		
			x	y	z
1	6	0	0.603296	0.347427	2.588732
2	6	0	-0.603291	-0.347513	2.588731
3	7	0	-1.210477	-0.69078	1.446702
4	6	0	-0.617831	-0.346414	0.299309
5	6	0	0.617824	0.346358	0.29931
6	7	0	1.210476	0.690709	1.446704
7	6	0	1.29922	0.752182	-0.993607
8	6	0	-1.299234	-0.75222	-0.99361
9	6	0	2.713358	1.312741	-0.808403
10	6	0	3.847343	0.38243	-0.510278
11	6	0	5.127573	0.933559	-0.331639
12	6	0	6.219444	0.11155	-0.063669
13	6	0	6.047768	-1.27464	0.027412
14	6	0	4.779201	-1.83317	-0.148904
15	6	0	3.684623	-1.008898	-0.415522
16	6	0	-2.713383	-1.312749	-0.808406
17	6	0	-3.847345	-0.382413	-0.510274
18	8	0	-2.900445	-2.512118	-0.952117
19	6	0	-5.127588	-0.933513	-0.331636
20	6	0	-6.219439	-0.111479	-0.063656
21	6	0	-6.047729	1.274706	0.027433
22	6	0	-4.779149	1.833207	-0.148882
23	6	0	-3.684591	1.00891	-0.415509
24	8	0	2.90038	2.512126	-0.952033
25	1	0	1.094012	0.634215	3.515351
26	1	0	-1.094001	-0.634314	3.515349
27	1	0	1.318388	-0.094798	-1.69043
28	1	0	0.72211	1.548157	-1.478447
29	1	0	-1.318382	0.094763	-1.69043
30	1	0	-0.72214	-1.548205	-1.478452
31	1	0	5.240339	2.009888	-0.406374
32	1	0	7.204451	0.547716	0.074398
33	1	0	6.899329	-1.916205	0.235256
34	1	0	4.641387	-2.907971	-0.078005
35	1	0	2.70629	-1.460368	-0.542899
36	1	0	-5.24038	-2.009839	-0.406378
37	1	0	-7.204455	-0.547623	0.074411
38	1	0	-6.899274	1.91629	0.235285
39	1	0	-4.641309	2.908004	-0.077976
40	1	0	-2.706248	1.460358	-0.542885

Table S28. Result of TD-DFT calculation for **ortho-L** (keto-keto form) at the S_0 geometry

Excited State	Spin Multiplicity	Energy / eV	Wavelength / nm	*f*	Composition	Coefficient
1	Singlet-A	3.7159	333.66	0.0002		
					HOMO-6 -> LUMO	0.19635
					HOMO-1 -> LUMO+1	0.4483
					HOMO -> LUMO	0.47013
2	Singlet-A	3.7189	333.39	0.0001		
					HOMO-6 -> LUMO+1	0.19332
					HOMO-1 -> LUMO	0.48837
					HOMO -> LUMO+1	0.42963
3	Singlet-A	3.9707	312.25	0.0036		
					HOMO-6 -> LUMO+2	-0.25629
					HOMO -> LUMO+2	0.65298

Table S29. Optimized geometry of **ortho-B** at the S_0 state

Center Number	Atomic Number	Coordinates (Angstroms)		
		x	y	z
1	6	0.682004	-1.685658	0.009693
2	6	-0.681977	-1.685668	-0.009794
3	7	-1.386638	-0.518561	-0.033544
4	6	-0.72755	0.663393	-0.068342
5	6	0.727549	0.6634	0.068268
6	7	1.386649	-0.518545	0.033481
7	6	1.451717	1.85628	0.314665
8	5	3.026063	-0.524537	-0.007227
9	6	-1.45173	1.85626	-0.314759
10	6	2.73549	1.787605	0.835805
11	6	3.426426	2.956794	1.427961
12	8	3.373744	0.65023	0.915047
13	6	3.027296	4.275826	1.145469
14	6	3.694178	5.356708	1.719075
15	6	4.765152	5.140094	2.591942
16	6	5.172431	3.833841	2.876453
17	6	4.51576	2.751034	2.293175
18	6	-2.735506	1.787559	-0.835893
19	6	-3.426455	2.956729	-1.428064
20	8	-3.373748	0.650177	-0.915103
21	6	-4.515728	2.750948	-2.293349
22	6	-5.172404	3.833744	-2.876642
23	6	-4.765194	5.140006	-2.59207
24	6	-3.694287	5.35664	-1.719126
25	6	-3.027397	4.275769	-1.145506
26	5	-3.026047	-0.524556	0.007213
27	6	3.640938	-0.090202	-1.475938
28	6	5.01537	0.294863	-1.496861
29	6	5.62067	0.752483	-2.675194
30	6	4.925147	0.85884	-3.8794
31	6	3.593765	0.446773	-3.874623
32	6	2.951322	-0.025517	-2.718332
33	6	1.518617	-0.487314	-2.933911
34	6	5.929917	0.221012	-0.283751
35	6	5.584183	1.395811	-5.128473
36	6	3.531921	-1.91576	0.70076
37	6	4.046668	-3.022662	-0.034425
38	6	4.494604	-4.177302	0.627617
39	6	4.451619	-4.310597	2.014545
40	6	3.89696	-3.252517	2.735258
41	6	3.435008	-2.0825	2.115781
42	6	2.822572	-1.052422	3.052233
43	6	4.137028	-3.067903	-1.550491
44	6	4.981668	-5.544202	2.707056
45	6	-3.531942	-1.915808	-0.700687
46	6	-3.43508	-2.082619	-2.115703
47	6	-3.897109	-3.252642	-2.735113
48	6	-4.4518	-4.31066	-2.014335
49	6	-4.494724	-4.177304	-0.627409
50	6	-4.046708	-3.022657	0.034565
51	6	-4.137017	-3.067828	1.550636
52	6	-2.822628	-1.052613	-3.052223
53	6	-4.981957	-5.544264	-2.706764
54	6	-3.640877	-0.090138	1.475919
55	6	-2.95123	-0.02545	2.718304
56	6	-3.593611	0.446927	3.874583
57	6	-4.924972	0.859092	3.879364
58	6	-5.620526	0.752713	2.675185
59	6	-5.015278	0.294997	1.496853
60	6	-5.92987	0.221127	0.283779
61	6	-1.518555	-0.48735	2.933862
62	6	-5.583892	1.396242	5.12842
63	1	1.259299	-2.599101	0.017785
64	1	-1.259265	-2.599115	-0.017914
65	1	0.931091	2.798639	0.315425
66	1	-0.931112	2.798624	-0.315561
67	1	2.212823	4.465679	0.454546
68	1	3.381463	6.368883	1.480527
69	1	5.281448	5.9835	3.040854
70	1	6.006037	3.657308	3.549643
71	1	4.835817	1.73752	2.503774
72	1	-4.835736	1.737427	-2.503988
73	1	-6.00596	3.657197	-3.549889
74	1	-5.281495	5.983403	-3.040994
75	1	-3.381631	6.368822	-1.480527
76	1	-2.212982	4.465632	-0.454519
77	1	6.674896	1.02395	-2.647221
78	1	3.031163	0.478119	-4.806003
79	1	1.312347	-0.570254	-4.004487
80	1	1.317116	-1.46785	-2.495321
81	1	0.78309	0.214756	-2.527547
82	1	5.895984	1.147702	0.298615
83	1	5.673575	-0.59527	0.392778
84	1	6.965902	0.077873	-0.607871
85	1	6.64128	1.113667	-5.176126
86	1	5.092319	1.022705	-6.032513
87	1	5.539074	2.492229	-5.160111
88	1	4.88263	-5.00097	0.031443
89	1	3.807387	-3.340818	3.816605
90	1	3.496539	-0.209745	3.231128
91	1	1.88849	-0.633682	2.670131
92	1	2.603666	-1.513799	4.019881
93	1	4.923103	-2.414885	-1.939326
94	1	4.357174	-4.088452	-1.878168
95	1	3.209191	-2.759455	-2.038005
96	1	4.924836	-6.423443	2.057419
97	1	6.034172	-5.415315	2.9908
98	1	4.422434	-5.760829	3.623151
99	1	-3.80757	-3.341	-3.816458
100	1	-4.882755	-5.000932	-0.031183
101	1	-4.357115	-4.08837	1.878369
102	1	-3.209184	-2.759315	2.038108
103	1	-4.923113	-2.414824	1.939457
104	1	-1.888534	-0.633867	-2.670159
105	1	-2.603745	-1.514054	-4.019846
106	1	-3.496581	-0.209933	-3.231164
107	1	-6.034636	-5.415542	-2.989936
108	1	-4.423154	-5.760635	-3.62318
109	1	-4.924619	-6.423597	-2.057294
110	1	-3.030993	0.478252	4.805955
111	1	-6.674737	1.024234	2.647229
112	1	-6.965844	0.077995	0.607942
113	1	-5.895962	1.147809	-0.298604
114	1	-5.673557	-0.595166	-0.392747
115	1	-1.317123	-1.467891	2.495257
116	1	-0.782988	0.21468	2.527499
117	1	-1.31228	-0.570318	4.004435
118	1	-5.093558	1.021232	6.032509
119	1	-5.536458	2.492532	5.161171
120	1	-6.641617	1.116297	5.174923

Table S30. Result of TD-DFT calculation for **ortho-B** at the S_0 geometry

Excited State	Spin Multiplicity	Energy / eV	Wavelength / nm	*f*	Composition	Coefficient
1	Singlet-A	2.3126	536.12	0.0163		
					HOMO-4 -> LUMO	0.14857
					HOMO-2 -> LUMO	0.55097
					HOMO -> LUMO	-0.40924
2	Singlet-A	2.3188	534.7	0.001		
					HOMO-1 -> LUMO	0.69734
3	Singlet-A	2.3773	521.54	0.0456		
					HOMO-5 -> LUMO	-0.11592
					HOMO-4 -> LUMO	-0.17347
					HOMO-2 -> LUMO	0.42948
					HOMO -> LUMO	0.51561

Table S31. S_1-state energy for each S_0 geometry of the complexes with different functionals[a]

Compound	Functional	Energy / eV	Wavelength / nm
para-B	B3LYP	1.9559	633.90
	CAM-B3LYP	2.2714	545.85
para-BMeO	B3LYP	1.8082	685.69
	CAM-B3LYP	2.2195	558.61
ortho-B	B3LYP	2.3126	536.12
	CAM-B3LYP	2.7303	454.10

[a]The 6-31+G(d,p) basis set was employed for all calculations.